15. SITE 1087[1]

Shipboard Scientific Party[2]

HOLE 1087A

Position: 31°27.8813′S, 15°18.6541′E

Start hole: 0210 hr, 3 October 1997

End hole: 2225 hr, 3 October 1997

Time on hole: 20.25 hr

Seafloor (drill pipe measurement from rig floor, mbrf): 1383.3

Total depth (drill pipe measurement from rig floor, mbrf): 1638.5

Distance between rig floor and sea level (m): 11.7

Water depth (drill pipe measurement from sea level, m): 1371.6

Penetration (mbsf): 255.2

Coring totals:
Type: APC
Number: 27
Cored: 255.2 m
Recovered: 252.38 m (98.89%)

Lithology:
Unit I: foraminifer-nannofossil ooze, foraminifer-rich nannofossil ooze, foraminifer-bearing nannofossil ooze, and nannofossil ooze

HOLE 1087B

Position: 31°27.8975′S, 15°18.6541′E

Start hole: 2225 hr, 3 October 1997

End hole: 0340 hr, 4 October 1997

Time on hole: 5.25 hr

Seafloor (drill pipe measurement from rig floor, mbrf): 1383.5

Total depth (drill pipe measurement from rig floor, mbrf): 1456

Distance between rig floor and sea level (m): 11.7

Water depth (drill pipe measurement from sea level, m): 1371.8

Penetration (mbsf): 72.5

Coring totals:
Type: APC
Number: 8
Cored: 72.5 m
Recovered: 74.83 m (103.21%)

Lithology:
Unit I: foraminifer-nannofossil ooze, foraminifer-rich nannofossil ooze, foraminifer-bearing nannofossil ooze, and nannofossil ooze

HOLE 1087C

Position: 31°27.9137′S, 15°18.6541′E

Start hole: 0340 hr, 4 October 1997

End hole: 0705 hr, 6 October 1997

Time on hole: 51.42 hr

Seafloor (drill pipe measurement from rig floor, mbrf): 1385.9

Total depth (drill pipe measurement from rig floor, mbrf): 1877.8

Distance between rig floor and sea level (m): 11.7

Water depth (drill pipe measurement from sea level, m): 1374.2

Penetration (mbsf): 491.9

Coring totals:
Type: APC
Number: 27
Cored: 248.60 m
Recovered: 255.01 m (102.58%)

Type: XCB
Number: 26
Cored: 243.30 m
Recovered: 223.29 m (91.78%)

Lithology:
Unit I: foraminifer-nannofossil ooze, foraminifer-rich nannofossil ooze, foraminifer-bearing nannofossil ooze, and nannofossil ooze
Unit II: foraminifer-bearing and foraminifer-rich nannofossil ooze

HOLE 1087D

Position: 31°27.9299′S, 15°18.6541′E

Start hole: 0705 hr, 6 October 1997

End hole: 0700 hr, 7 October 1997

Time on hole: 23.92 hr

Seafloor (drill pipe measurement from rig floor, mbrf): 1383.5

Total depth (drill pipe measurement from rig floor, mbrf): 1584.8

Distance between rig floor and sea level (m): 11.7

Water depth (drill pipe measurement from sea level, m): 1371.8

Penetration (mbsf): 201.3

Coring totals:
Type: APC
Number: 13
Cored: 119.20 m
Recovered: 121.04 m (101.54%)

Type: XCB
Number: 1
Cored: 9.60 m
Recovered: 9.88 m (102.92%)

Lithology:
Unit I: foraminifer-nannofossil ooze, foraminifer-rich nannofossil ooze, foraminifer-bearing nannofossil ooze, and nannofossil ooze

[1]Wefer, G., Berger, W.H., Richter, C., et al., 1998. *Proc. ODP, Init. Repts.*, 175: College Station, TX (Ocean Drilling Program).

[2]Shipboard Scientific Party is given in the list preceding the Table of Contents.

Principal results: Site 1087 is located in the southernmost area of the Cape Basin in 1371 m deep water. The primary objective for drilling at this site is to explore the Neogene history of the Benguela Current in the Southern Cape Basin and to detect possible Agulhas Current influences. We expect to obtain information about the supply of warm water from the Indian Ocean, through the Agulhas Retroflection, and from the Subtropical Convergence Zone, which are nearby. Both warm-water and cold-water eddies can be shed from the retroflection and the front, but the position of the Subtropical Convergence Zone and the transport by the Benguela Current will be crucial in determining which type of eddy is more likely to reach the site. The site also is located close to the continent and should detect upwelling signals and signals from continental climates, as well as sea-level changes.

Four holes were cored with the advanced hydraulic piston corer/extended core barrel (APC/XCB) at Site 1087 to a maximum depth of 492 meters below seafloor (mbsf), which recovered a relatively continuous section down to 430 mbsf spanning the last 9 m.y. Hole 1087A was cored with the APC to 255.2 mbsf, and Hole 1087B was cored to 72.5 mbsf. Hole 1087C was cored with the APC to 248.60 mbsf and was extended with the XCB to 491.9 mbsf. The hole was logged with the seismostratigraphic suite. Logging was aborted after the logging tool got stuck and operations had to be terminated at Hole 1087C. Hole 1087D was drilled from 0 to 72.5 mbsf and cored to 201.3 mbsf in continuation of Hole 1087B. This hole ended Leg 175 operations with a total record-setting recovery of 8003.23 m.

Sedimentation rates range from 20 to 70 m/m.y. The bottom 70 m contain a middle Miocene to lower Oligocene/upper Eocene package interrupted by at least two major discontinuities. The sediments form two lithostratigraphic units that are composed of nannofossil ooze with varying abundances of clay and foraminifers. The sediments strongly resemble the lithologies observed at Sites 1086 and 1085. The sequence most likely contains various unconformities. The uppermost lithostratigraphic unit (0–425 mbsf) consists of nannofossil ooze with varying amounts of foraminifers. Sandy nannofossil foraminifer ooze is present in 50- to 100-cm-thick beds in the upper 45 m. These beds have generally sharp bases, grade upward into more clay-rich, olive foraminifer nannofossil ooze, and are interpreted as either turbidites or winnowed layers. The underlying unit (425–492 mbsf) comprises 2- to 100-cm-thick horizons of foraminifer-bearing and foraminifer-rich nannofossil ooze. A large unconformity is identified by an erosional contact at 450 mbsf and by biostratigraphic evidence. Below the erosional contact, fine laminations are present, which are microfolded with sharp upper and lower contacts.

The detrital component is dominated by clay and trace abundances of silt-sized, subangular mono- and polycrystalline quartz grains. Pyrite is present as silt-sized aggregates of euhedral crystals or framboids.

A preliminary biostratigraphy was developed using calcareous nannofossils and planktonic foraminifers. The biogenic component of both lithostratigraphic units consists of abundant to very abundant nannofossils. Foraminifers are abundant to few. Siliceous spicules, dinoflagellate cysts, and radiolarian tests are present in trace amounts in upper Pliocene and Pleistocene sediments only.

Radiolarian species indicate generally low productivity under subtropical warm-water conditions. The radiolarian assemblages that are characterized by common *Cycladophora davisiana* suggest upwelling conditions for samples from 60 to 70 mbsf. The occurrence of an Antarctic species at 112 mbsf indicates an influence of cooler water masses.

As at Site 1085, the upper Pliocene sediment at Site 1087 contains an interval with a mixed/*Thalassiothrix antarctica*–rich assemblage composed of Southern Ocean and warm-oceanic species, with an approximate age of 1.9–2.8 Ma. Dinoflagellate cysts are common below 213 mbsf and between 262 and 338 mbsf.

APC cores experienced a significant coring-induced remagnetization with a radial-inward direction. Only magnetic inclinations showed distinct polarity biases after alternating-field (AF) demagnetization at 20 mT, which allowed an interpretation of the magnetic polarity sequence from the Brunhes (C1n) Chron to the Gilbert (C2A) Chron (~ 4 Ma).

Magnetic susceptibility and gamma-ray attenuation porosity evaluator (GRAPE) wet bulk density data were measured at 5- and 10-cm intervals. The correlation of features present in the physical properties measurements at adjacent holes were used to demonstrate completeness of the stratigraphic sequence between 0 and 214 meters composite depth (mcd).

Sediments are carbonate rich and organic carbon poor. Interstitial water chemistry is controlled dominantly by the high carbonate and low organic carbon concentrations in the sediment, which results in modest variations in the chemical gradients of many dissolved species. Alkalinity rises to a broad maximum of ~30 mM between 60 and 126 mbsf and subsequently decreases downhole. Sulfate is not completely consumed until 60 mbsf. Carbonate and phosphate precipitation reactions throughout the sequence also are inferred from the profiles of dissolved calcium, magnesium, and phosphate. Among the three Cape Basin sites, 1087 is most similar to Site 1085 in its geochemical profiles.

Logging in Hole 1087C encountered serious problems when the tool got stuck while entering the pipe after the first run. Good-quality logs were recorded with the seismostratigraphy tool string. In the upper 300 m of the logged interval, downhole measurements show very homogeneous patterns. The lower part of the logged interval is characterized by more variations in physical records related to the carbonate vs. detrital content.

Site 1087 is the southernmost site of a north–south transect along the west African coast, from the Congo to South Africa. Sediments at this site were deposited continuously over the last 9 m.y. and will permit the reconstruction of the advection of water masses from the Indian Ocean and the Subantarctic Region. It also will provide important new data about early carbonate diagenesis and the processes involved in sediment redeposition on the continental slope.

BACKGROUND AND OBJECTIVES

For a discussion of the background and objectives for Site 1087 see "Background and Objectives" section, "Site 1086" chapter (this volume).

OPERATIONS

Hole 1087A (Proposed Site SCB-1)

The 19-nmi voyage to Site 1087 was accomplished at an average speed of 12.6 kt. The vessel approached the Global Positioning System coordinates of the site, and a beacon was deployed at 0210 hr on 3 October. Hole 1087A was spudded with the APC at 0600 hr, and the seafloor depth was estimated from the recovery of the first core at 1371.6 meters below sea level (mbsl). APC coring advanced without incident to 255.2 mbsf (Table 1; also see expanded coring summary table on CD-ROM, back pocket, this volume), which was considered refusal depth for piston coring, with 98.9% recovery. Cores were oriented starting with Core 175-1087A-3H. Adara heat-flow measurements were taken at 46.2 mbsf (5H), 65.2 mbsf (7H), 93.7 mbsf (10H), and 122.2 mbsf (13H). The drill string was pulled out of the hole with the bit clearing the seafloor at 2225 hr on 3 October, thereby ending operations at Hole 1087A.

Hole 1087B

The vessel was offset 30 m to the south, and Hole 1087B was spudded with the APC at 2317 hr. The recovery of the first core established the seafloor depth at 1371.8 mbsl. APC coring advanced without incident to 72.5 mbsf, with 103.4% recovery (Table 1). Cores were oriented starting with Core 175-1087B-3H. The bit was pulled out of the hole and cleared the seafloor at 0340 hr on 4 October, thereby ending Hole 1087B.

Hole 1087C

Hole 1087C was spudded with the APC at 0425 hr. The recovery of the first core established the seafloor depth at 1376.2 mbsl. Piston

Table 1. Coring summary for Site 1087.

Core	Date (Oct 1997)	Time (UTC)	Interval (mbsf)	Length cored (m)	Length recovered (m)	Recovery (%)
175-1087A-						
1H	3	0605	0.0-8.2	8.2	8.26	100.7
2H	3	0640	8.2-17.7	9.5	10.02	105.5
3H	3	0710	17.7-27.2	9.5	10.10	106.3
4H	3	0740	27.2-36.7	9.5	9.61	101.2
5H	3	0825	36.7-46.2	9.5	9.90	104.2
6H	3	0855	46.2-55.7	9.5	9.97	104.9
7H	3	0935	55.7-65.2	9.5	10.06	105.9
8H	3	1005	65.2-74.7	9.5	9.19	96.7
9H	3	1030	74.7-84.2	9.5	9.91	104.3
10H	3	1115	84.2-93.7	9.5	9.52	100.2
11H	3	1140	93.7-103.2	9.5	9.77	102.8
12H	3	1210	103.2-112.7	9.5	9.82	103.4
13H	3	1300	112.7-122.2	9.5	10.20	107.4
14H	3	1330	122.2-131.7	9.5	9.63	101.4
15H	3	1400	131.7-141.2	9.5	10.07	106.0
16H	3	1435	141.2-150.7	9.5	9.68	101.9
17H	3	1505	150.7-160.2	9.5	8.94	94.1
18H	3	1540	160.2-169.7	9.5	8.44	88.8
19H	3	1610	169.7-179.2	9.5	10.21	107.5
20H	3	1640	179.2-188.7	9.5	9.51	100.1
21H	3	1715	188.7-198.2	9.5	10.07	106.0
22H	3	1750	198.2-207.7	9.5	8.56	90.1
23H	3	1820	207.7-217.2	9.5	5.82	61.3
24H	3	1855	217.2-226.7	9.5	10.03	105.6
25H	3	1925	226.7-236.2	9.5	9.57	100.7
26H	3	2005	236.2-245.7	9.5	6.02	63.4
27H	3	2040	245.7-255.2	9.5	9.50	100.0
Coring totals:				255.2	252.38	98.9
175-1087B-						
1H	3	2330	0.0-6.0	6.0	6.08	101.3
2H	4	0005	6.0-15.5	9.5	9.91	104.3
3H	4	0035	15.5-25.0	9.5	9.87	103.9
4H	4	0105	25.0-34.5	9.5	10.00	105.3
5H	4	0130	34.5-44.0	9.5	9.93	104.5
6H	4	0200	44.0-53.5	9.5	9.93	104.5
7H	4	0235	53.5-63.0	9.5	9.54	100.4
8H	4	0305	63-72.5	9.5	9.57	100.7
Coring totals:				72.5	74.83	103.2
175-1087C-						
1H	4	0435	0-1.6	1.6	1.68	105.0
2H	4	0500	1.6-11.1	9.5	9.78	102.9
3H	4	0525	11.1-20.6	9.5	9.27	97.6
4H	4	0600	20.6-30.1	9.5	9.94	104.6
5H	4	0630	30.1-39.6	9.5	9.91	104.3
6H	4	0700	39.6-49.1	9.5	9.60	101.1
7H	4	0735	49.1-58.6	9.5	9.98	105.1
8H	4	0800	58.6-68.1	9.5	10.00	105.3
9H	4	0830	68.1-77.6	9.5	9.79	103.1
10H	4	0900	77.6-87.1	9.5	10.02	105.5
11H	4	0930	87.1-96.6	9.5	9.41	99.1
12H	4	1000	96.6-106.1	9.5	9.72	102.3
13H	4	1025	106.1-115.6	9.5	9.63	101.4
14H	4	1055	115.6-125.1	9.5	10.07	106.0
15H	4	1120	125.1-134.6	9.5	9.62	101.3
16H	4	1150	134.6-144.1	9.5	9.74	102.5
17H	4	1220	144.1-153.6	9.5	9.85	103.7
18H	4	1250	153.6-163.1	9.5	9.91	104.3
19H	4	1325	163.1-172.6	9.5	9.87	103.9
20H	4	1355	172.6-182.1	9.5	9.04	95.2
21H	4	1430	182.1-191.6	9.5	9.53	100.3
22H	4	1505	191.6-201.1	9.5	9.94	104.6
23H	4	1540	201.1-210.6	9.5	9.64	101.5
24H	4	1615	210.6-220.1	9.5	9.44	99.4
25H	4	1650	220.1-229.6	9.5	10.07	106.0
26H	4	1725	229.6-239.1	9.5	10.03	105.6
27H	4	1800	239.1-248.6	9.5	9.53	100.3
28X	4	1850	248.6-254.9	6.3	9.85	156.3
29X	4	1925	254.9-261.2	6.3	7.55	119.8
30X	4	1955	261.2-270.8	9.6	9.81	102.2
31X	4	2030	270.8-280.4	9.6	9.71	101.1
32X	4	2105	280.4-290	9.6	9.85	102.6
33X	4	2140	290.0-299.7	9.7	9.73	100.3
34X	4	2215	299.7-309.3	9.6	9.70	101.0
35X	4	2250	309.3-318.9	9.6	9.89	103.0
36X	4	2320	318.9-328.5	9.6	9.82	102.3
37X	4	2355	328.5-338.2	9.7	9.79	100.9
38X	5	0035	338.2-347.8	9.6	9.63	100.3
39X	5	0135	347.8-357.4	9.6	8.54	89.0
40X	5	0240	357.4-367.1	9.7	8.68	89.5
41X	5	0340	367.1-376.7	9.6	8.24	85.8
42X	5	0415	376.7-386.3	9.6	9.56	99.6
43X	5	0500	386.3-396.0	9.7	8.61	88.8
44X	5	0550	396-405.6	9.6	9.68	100.8
45X	5	0640	405.6-415.2	9.6	0.05	0.5
46X	5	0725	415.2-424.8	9.6	9.69	100.9
47X	5	0815	424.8-434.5	9.7	8.34	86.0
48X	5	0910	434.5-444.1	9.6	8.95	93.2
49X	5	1010	444.1-453.8	9.7	6.38	65.8
50X	5	1120	453.8-463.4	9.6	4.76	49.6
51X	5	1245	463.4-473.1	9.7	9.8	101.0
52X	5	1435	473.1-482.7	9.6	6.95	72.4
53X	5	1605	482.7-491.9	9.2	9.73	105.8
Coring totals:				491.9	478.30	97.2
175-1087D-						
1-0	6	1145	0.0-72.5	0.0	0.00	N/A
1H	6	1225	72.5-82.0	9.5	9.98	105.1
2H	6	1300	82.0-91.5	9.5	8.10	85.3
3H	6	1330	91.5-101.0	9.5	9.18	96.6
4H	6	1400	101.0-110.5	9.5	9.52	100.2
5H	6	1435	110.5-120.0	9.5	10.23	107.7
6H	6	1505	120.0-129.5	9.5	9.46	99.6
7H	6	1535	129.5-139.0	9.5	10.20	107.4
8H	6	1610	139.0-148.5	9.5	9.50	100.0
9H	6	1645	148.5-158.0	9.5	10.15	106.8
10H	6	1720	158.0-167.5	9.5	9.91	104.3
11H	6	1750	167.5-177.0	9.5	9.99	105.2
12X	6	1840	177.0-186.6	9.6	9.88	102.9
13H	6	1910	186.6-195.3	8.7	8.77	100.8
14H	6	1955	195.3-201.3	6.0	6.05	100.8
Coring totals:				128.8	130.92	101.7

Notes: UTC = Universal Time Coordinated. An expanded version of this coring summary table that includes lengths and depths of sections and comments on sampling is included on CD-ROM (back pocket, this volume).

coring advanced to refusal at 248.6 mbsf (Table 1). Cores were oriented starting with Core 175-1087C-4H. The hole was extended with the extended core barrel (XCB) to 491.9 mbsf, with 91.8% recovery.

Logging Operations in Hole 1087C

In preparation for logging, an aluminum go-devil was dropped to ensure the opening of the lockable float valve. After the hole was flushed with a high-viscosity mud treatment, the drill string was pulled back to 442.8 mbsf, where the top drive was set back. The drill string was then placed at the logging depth of 85.8 mbsf. Logging operations began at 1930 hr on 5 October. The initial log was conducted with the seismostratigraphic suite (25.8 m long). This suite was made up of the spectral gamma-ray (NGT), long-spacing sonic (LSS), phasor dual-induction (DIT), and Lamont-Doherty high-resolution temperature (TLT) sondes. This tool string was deployed in the pipe at 2015 hr and logged the hole down to and then up from 487.1 mbsf.

While attempting to recover the logging tool string, the instrument hung up ~5 m inside the bit. Maximum overpull on the logging line was 1200 lbs. The logging tool string was eventually freed from the bit by pumping. The logging winch operator tried to work the tool into the drill string again by incrementally pulling on the logging line up to a maximum of 4000 lbs head tension. This time, the tool string became totally stuck in the bit and was unable to be worked up or down. Attempts to retrieve the logging tool string with the logging cable were given up, and the Kinley cutter and crimper tools were prepared. The Kinley crimper was dropped and followed by a Kinley hammer. The drill string was pulled out of the hole, with the bit clearing the plane of the rotary table at 0715 hr. The logging tool string was not recovered.

Hole 1087D

The vessel was offset 30 m to the south, and Hole 1087D was spudded at 1030 hr on 6 October. After drilling to 72.5 mbsf, piston coring was initiated. APC coring proceeded to 177.0 mbsf (Table 1), which required the use of the last full-sized liner. A sole XCB core was then taken from 177.0 to 186.6 mbsf and recovered 9.88 m

(102.9%). This core used the last liner of any length whatsoever on the vessel. The hole was then completed to a depth of 201.3 mbsf with two piston cores, which were obtained without liners, and recovered 100%. The total piston cored interval was 119.2 mbsf, with 121.04 m recovered (101.5%). The last core gave a total leg recovery of 8003.23 m. The drill string was then pulled out of the hole, with the bit clearing the seafloor at 2140 hr. The beacon was recovered at 2215 hr. The bit was at the rotary table at 0145 hr on 7 October. At 0700 hr on 7 October, the vessel departed the last site of Leg 175.

SITE GEOPHYSICS

For a discussion of site geophysics at Site 1087, see "Site Geophysics" section, "Site 1086" chapter (this volume).

LITHOSTRATIGRAPHY

Description of Lithostratigraphic Units

The sediments drilled at Site 1087 exhibited only a few minor gas expansion cracks. No flow-in was observed. Core disturbance is minimal. Material cored with the extended core barrel below Core-175-1087C-28X consisted of drilling biscuits embedded in drill mud. Sediments from Site 1087 form two lithostratigraphic units composed of nannofossil ooze with varying abundances of clay and foraminifers (Fig. 1). The sediments recovered from Site 1087 are lithologically similar to sediments from Sites 1086 and 1085.

Unit I

Intervals: 175-1087A-1H through 175-1087A-27H; 175-1087B-1H through 175-1087B-23H; 175-1087C-1H through 175-1087C-47X
Age: early Pleistocene to early Oligocene
Depth: Hole 1087A: 0–255.2 mbsf; Hole 1087B: 0–72.5 mbsf; Hole 1087C: 0–424.8 mbsf; Hole 1087D: 0–201.3 mbsf

Unit I is composed of light gray (5Y 7/1), pale olive (5Y 6/3) and light olive-gray (5Y 6/2) foraminifer-nannofossil ooze, foraminifer-rich nannofossil ooze, foraminifer-bearing nannofossil ooze, and nannofossil ooze. Sandy nannofossil-foraminifer ooze is present in 50- to 100-cm-thick beds in the upper 45 m of Holes 1087A, 1087B, and 1087C. These beds generally have sharp bases and grade upward from foraminifer sands into more clay-rich, olive-colored foraminifer-nannofossil ooze. The tops of these layers are often intensely bioturbated. These beds are interpreted as turbidites or the products of winnowing. All cores are moderately bioturbated, and burrows range in diameter from 1 mm to over 1 cm.

Some larger burrows are dark gray, contain abundant pyrite, and are frequently filled with silt- to sand-sized foraminifer tests. Gray blebs with abundant pyrite are found disseminated throughout Cores 175-1087C-32X through 38X. Cores 40X, 41X, and 43X contain pyrite nodules ranging in diameter from 1 mm to 2 cm. Occasionally, *Zoophycos* traces are identified. Intervals of different colored sediment range in thickness from 40 to 100 cm and grade into one another over 15 to 20 cm. Small, finely dispersed fine sand-sized pyrite grains are ubiquitous below Core 175-1086A-16H. The boundary between Units I and II occurs between Cores 175-1087C-46X and 47X. Across the boundary, light greenish gray (5GY 7/1) nannofossil ooze changes to foraminifer-bearing nannofossil ooze that exhibits rapid changes in color, high abundances of pyrite in darker colored sections, and microfaulted thinly laminated sections. This lithostratigraphic contact coincides with the disconformity identified from biostratigraphy ("Biostratigraphy and Sedimentation Rates" section, this chapter).

Unit II

Interval: 175-1087C-47X through 175-1087C-53X
Age: early Oligocene to late Eocene
Depth: Hole 1087C: 424.8–491.9 mbsf

Unit II extends from Cores 175-1087C-47X to the bottom of the hole at 53X. It is composed of 2- to 100-cm-thick, light gray (5Y 7/2) greenish gray (5G 6/1), light olive-gray (5Y 5/1), light greenish gray (5G 7/1), brown (10YR 4/3), and brownish gray (10YR 6/1) intervals of foraminifer-bearing and foraminifer-rich nannofossil ooze. These intervals have bioturbated boundaries that grade over 2–10 cm (see Fig. 2). Intervals of thinly laminated sediments are common and often convolutely layered, microfaulted, and sometimes tightly folded. Contacts between intervals are sharp. Individual laminae have sharp upper and lower contacts and range in thickness from 1 to 3 mm. The top of Core 175-1087C-50X contains a large pyrite concretion surrounded by a 1-cm-thick brown (10YR 4/3) iron oxide–rich rim of foraminifer-bearing nannofossil ooze (see Fig. 3). The oxidized rim is interpreted as a secondary feature resulting from reoxidation of the outside of the pyrite nodule. Because the pyrite nodule must have grown under reducing conditions below the surface, it must have been exposed via oxygenated conditions later. Biostratigraphy indicates that there is a large disconformity between Cores 175-1087C-49X and 50X ("Biostratigraphy and Sedimentation Rates" section, this chapter), supporting the interpretation of an erosional contact near the stratigraphic level of the pyrite nodule. Below the erosional contact are fine laminae that are mircofolded with sharp upper and lower contacts (see Fig. 4). Cores 175-1087C-51X through 53X are composed of moderately bioturbated 10-cm-thick layers of light gray (5Y 7/2, N/8) carbonate-rich nannofossil oozes and light brownish gray (10YR 6/3) foraminifer-bearing nannofossil oozes. The contacts between these intervals are bioturbated and grade into one another over 2 cm.

Synthesis of Smear-Slide Analyses

The detrital component in sediments from Site 1087 is dominated by clay and trace abundances of silt-sized, subangular mono- and polycrystalline quartz grains. Authigenic minerals are rare or present in trace abundances. Pyrite is present as silt-sized aggregates of euhedral crystals or as framboids. Very fine-grained phosphate peloids are present in bioturbated beds in trace to few amounts in Cores 175-1087A-18H, 20H, 22H, and 25H. In Unit II, iron oxide minerals may be responsible for the brownish color, whereas apatites may be responsible for the yellowish color exhibited by the sediments. The biogenic component of both units consists of abundant to very abundant nannofossils. Foraminifers are abundant to few. The abundance of diatoms is few in Cores 175-1087A-8H and 10H. Siliceous spicules, dinoflagellate cysts, and radiolarian tests are present in trace amounts.

Spectrophotometry

Color reflectance data were measured every 4 cm for Holes 1087A, 1087B, 1087C, and 1087D (Figs. 5, 6). The total reflectance values range between 45% and 70% (Figs. 2, 3), reflecting the high average calcium carbonate contents at this site. The downcore variation in the total reflectance values shows high variability attributed in part to intervals of light coarse-grained foraminifer beds in the upper 50 mbsf (Figs. 2, 5) and to a low sedimentation rate (see "Biostratigraphy and Sedimentation Rates" section, this chapter). Total reflectance and the red/blue wavelength ratio at Hole 1087C display distinct features (see Fig. 6): There are high values of total reflectance between 100 and 120 mbsf and between 270 and 330 mbsf and pronounced low total reflectance values in the interval between 340 and 370 mbsf. Similar variations have been observed at Site 1085 (see

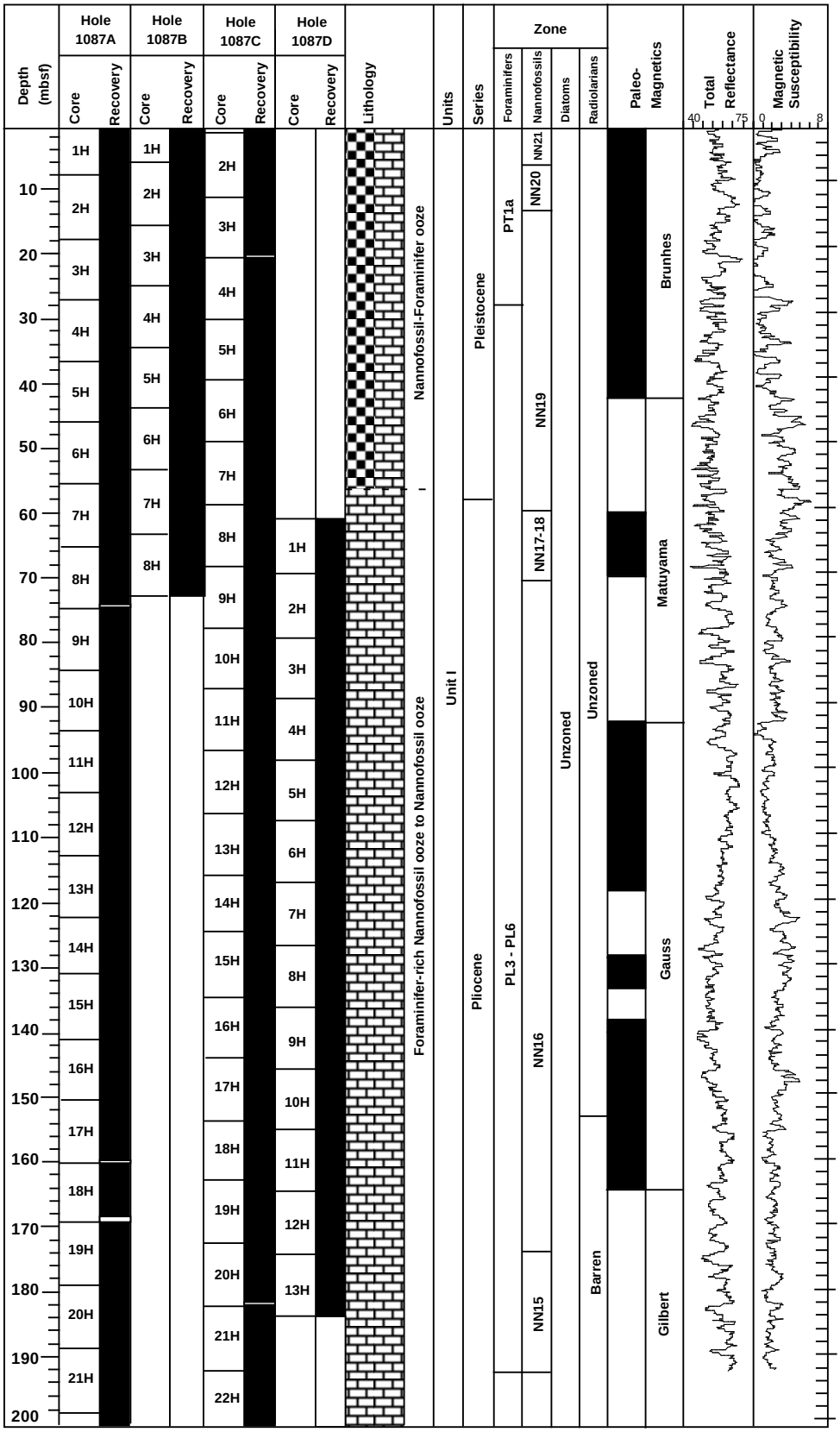

Figure 1. Composite stratigraphic section for Site 1087 showing core recovery in all holes, a simplified summary of lithology, age, total reflectance (400–700 nm), and magnetic susceptibility. (Continued next page.)

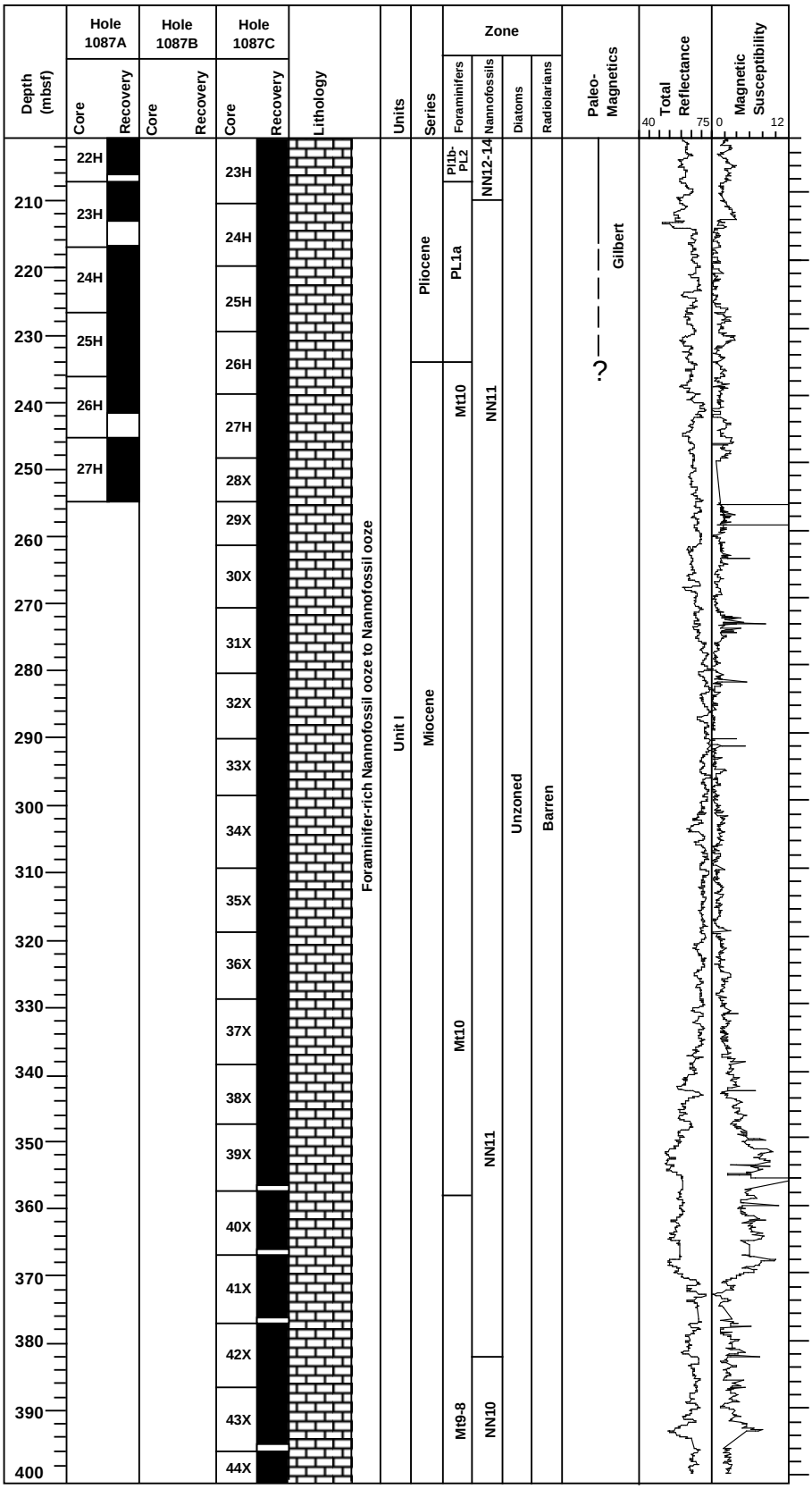

Figure 1 (continued).

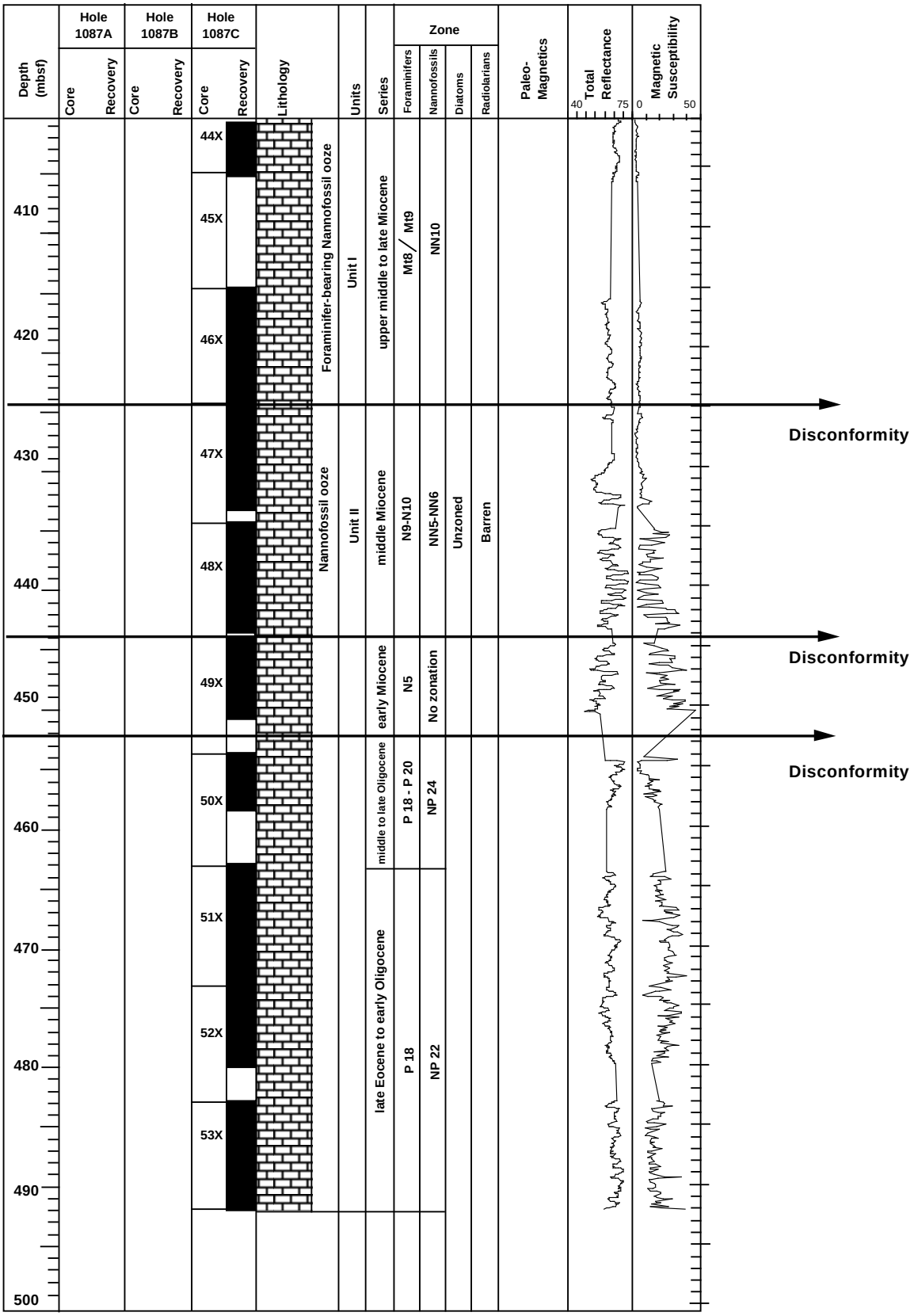

Figure 1 (continued).

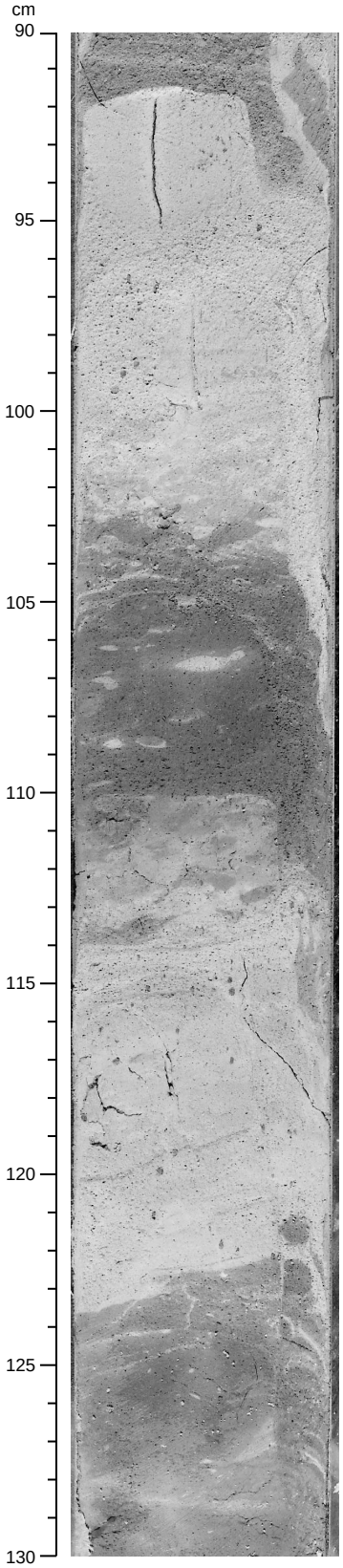

Figure 2. Close-up core photograph of Section 175-1087C-49X-4 showing bioturbated light greenish gray (5G 7/1) and brown (10YR 4/3) horizons of foraminifer-bearing and foraminifer-rich nannofossil ooze.

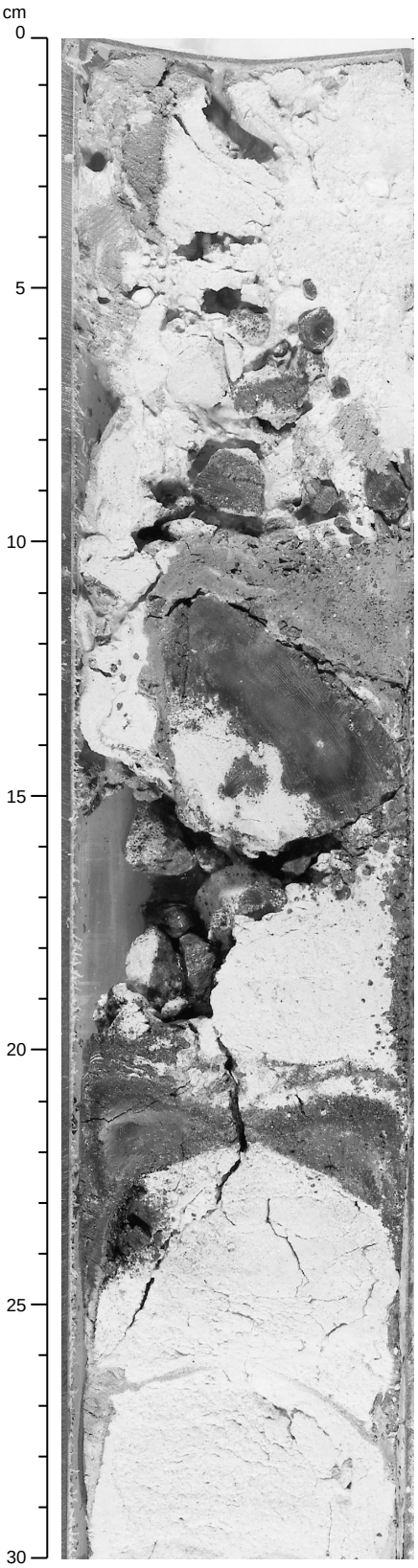

Figure 3. Close-up core photograph of the erosional contact in the top of Section 175-1087C-50X-1. A large pyrite nodule with a surrounding iron oxide–rich layer can also be observed (see text).

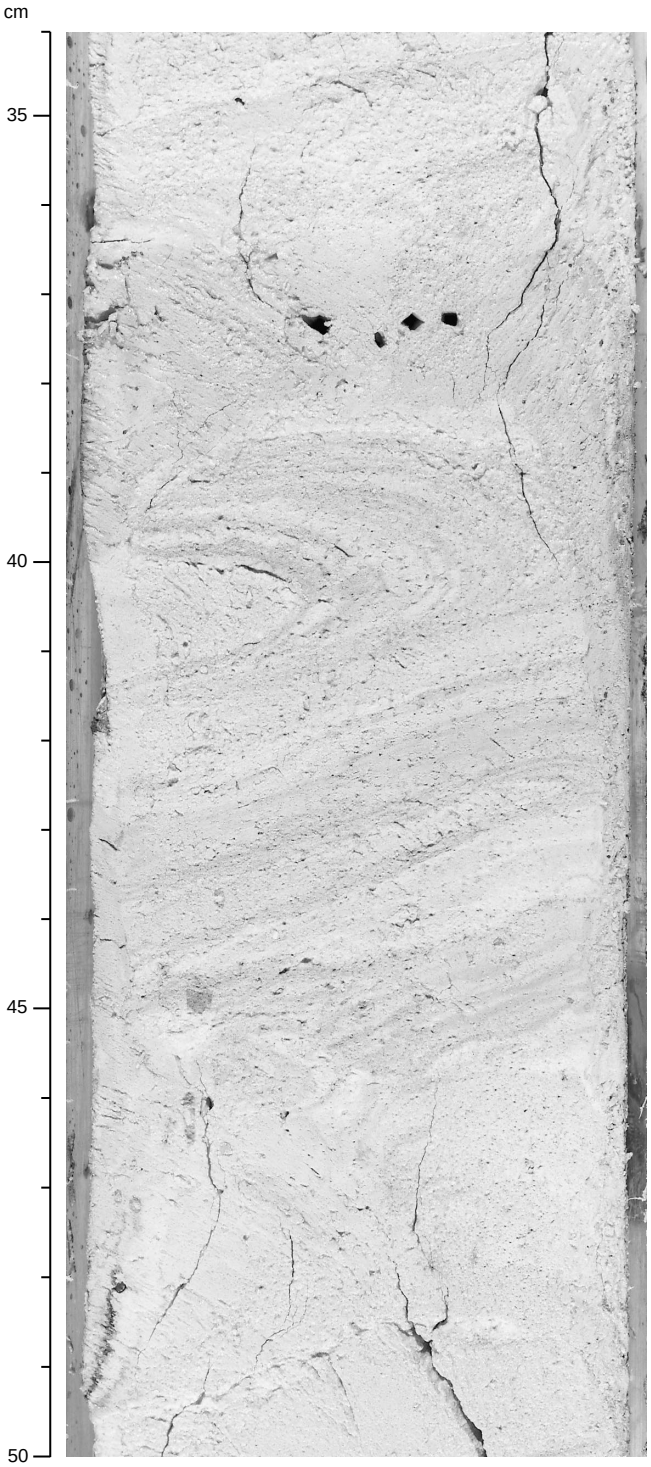

Figure 4. Close-up core photograph of the interval 175-1087C-50X-1, 34–50 cm, showing tightly folded laminae.

"Lithostratigraphy" section, "Site 1085" chapter, this volume). The red/blue ratio shows high values between 450 and the bottom of the core. These high values are thought to be associated to the presence of iron oxides in the sediments (see above).

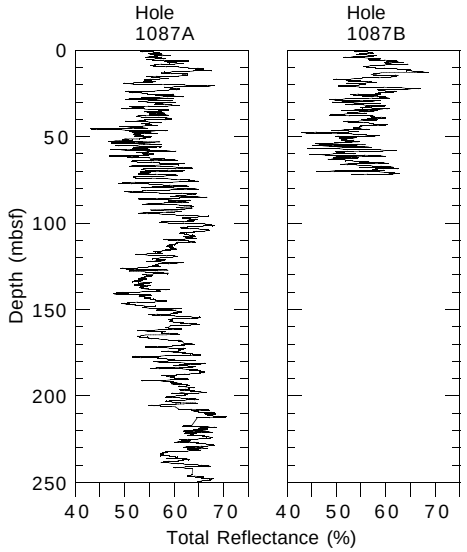

Figure 5. Downcore variations in the total reflectance at Holes 1087A and 1087B.

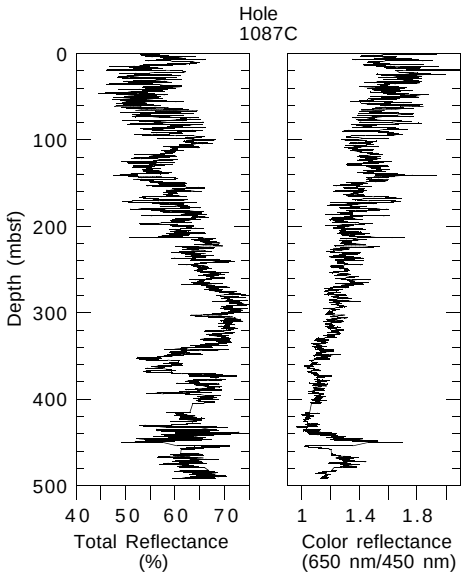

Figure 6. Downcore variations in the total reflectance and color reflectance (650 nm/450 nm) at Hole 1087C.

BIOSTRATIGRAPHY AND SEDIMENTATION RATES

Sediments recovered from Site 1087 represent a relatively continuous pelagic section down to 430 mbsf spanning the last 9 m.y. The bottom 70 m contains middle Miocene to early Oligocene sediment packages interrupted by at least two major discontinuities. The micropaleontological study was carried out on core-catcher samples from Holes 1087A and 1087C. Additional samples from within the cores were examined to improve the biostratigraphic resolution. A high-resolution biostratigraphy was developed using calcareous nannofossils and planktonic foraminifers. Sedimentation rates range

from 2 to 7 cm/k.y. Siliceous microfossils are present in the late Pliocene and Pleistocene only.

Calcareous Nannofossils

Calcareous nannofossils were examined in core-catcher samples from Hole 1087A. Additional samples from within the top six cores of Hole 1087A were studied close to datum events to improve the stratigraphic resolution of the Pleistocene interval. Core-catcher samples from Hole 1087C (Cores 175-1087A-26H through 51X-CC) were examined to resolve the stratigraphy of the bottom 300 m of Site 1087. Calcareous nannofossils are abundant and well preserved throughout the section.

At least three major discontinuities were identified within the bottom 70 m of Site 1087. This disturbed interval contains sediment packages of middle Miocene (Zone NN5; Sample 175-1087C-47X-CC) and Oligocene (Zones NP22–NP24; Sample 175-1087C-50X-CC and 51X-CC) origin. Above this disturbed bottom interval, the nannofossil-derived stratigraphy suggests a continuous sedimentation spanning the Pleistocene to the middle Miocene (Zones NN21–NN10) (Table 2). The following discussion will refer only to this undisturbed section of Site 1087.

Zone NN21

Subzone NN21b is missing from the top part of Hole 1087A. The Subzone NN21a/NN20 boundary was identified within Core 175-1087A-1H (between Sample 1H-3, 130 cm, and 1H-CC) at the mean depth of 6.2 mbsf.

Zone NN20

This interval of 0.2-m.y. duration terminates at 13.4 mbsf (between Samples 175-1087A-2H-3, 130 cm, and 2H-4, 140 cm), which is the mean depth of the last occurrence (LO) of the *Pseudoemiliania lacunosa* datum event.

Zone NN19

In addition to the zonal boundary events, four biohorizons were identified within this interval. Based on the downcore distribution of these datum events, a rather uniform sedimentation rate is inferred for the Pleistocene and upper part of the late Pliocene of Site 1087 (Fig. 7). The base of Zone NN19 was identified between Samples 175-1087A-6H-CC and 7H-CC at the mean depth of 60.9 mbsf.

Zones NN18–NN17

Zones NN18 and NN17 were combined because the LOs of both *Discoaster pentaradiatus* (NN18/NN17 zonal boundary event) and *D. surculus* (NN17/NN16 zonal boundary) were identified within the same sampling interval (between Samples 175-1087A-8H-CC and 9H-CC; 79.4 mbsf). A refined biostratigraphy based on a higher resolution sampling will be done on shore to precisely constrain the upper boundary of the short-duration Zone NN17 (from 2.45 to 2.55 Ma).

Zone NN16

This 1.27-m.y. interval is constrained between 79.4 and 174.14 mbsf and displays the highest sedimentation rates recorded for Site 1087 (7 cm/k.y.). In addition to the zonal boundary events, a biohorizon dated at 1.83 Ma was identified between Samples 175-1087A-10H-CC and 11H-CC (LO of *Discoaster tamalis*).

Zone NN15

The top of this interval is defined by the LO of *Reticulofenestra pseudoumbilica* (3.82 Ma), a datum event identified between Samples 175-1087A-18H-CC and 19H-CC. The Zone NN15/NN14 boundary is defined by the LO of *Amaurolithus tricorniculatus* (4.5 Ma), a datum identified at the mean depth of 193.6 mbsf (Samples 175-1087A-20H-CC through 21H-CC).

Zones NN14, NN13, and NN12

These zones were combined because of the sparse occurrence of diagnostic and zonal boundary species of Zone NN13 (*Ceratolithus* sp.). The first occurrence (FO) of *Discoaster asymmetricus*, which defines the Zone NN14/NN13 boundary, could not be properly identified because of the combination of coarse sampling resolution and low sedimentation rates (2 cm/k.y.). The base of this interval was found between Samples 175-1087A-22H-CC and 23H-CC (LO of *Discoaster quinqueramus;* 5.54 Ma).

Zone NN11

This 3.06-m.y. interval is defined as the range of *D. quinqueramus*. The range of *Amaurolithus amplificus* (LO between Samples 175-1087C-27H-CC and 28X-CC; FO between Samples 30X-CC

Table 2. Calcareous nannofossil datums at Holes 1087A and 1087C.

Event	Age (Ma)	Zone (base)		Core, section, interval (cm)		Depth (mbsf)		
		A	B	Top	Bottom	Top	Bottom	Mean
				175-1087A-	175-1087A-			
FO *Emiliania huxleyi*	0.26	NN21	CN15	1H-3, 130	1H-CC	4.30	8.21	6.26
LO *Gephyrocapsa caribbeanica* acme	0.26	NN21	CN15	1H-3, 130	1H-CC	4.30	8.21	6.26
LO *Pseudoemiliania lacunosa*	0.46	NN20	CN14b	2H-3, 130	2H-4, 140	12.70	14.10	13.40
LO Small *Gephyrocapsa* acme (Weaver, 1993)	0.6			2H-4, 140	2H-CC	14.10	18.17	16.14
LO *Reticulofenestra asanoi*	0.83			3H-5, 140	3H-CC	25.00	27.75	26.38
LO *Helicosphaera sellii*	1.25			4H-CC	5H-3, 10	36.71	39.80	38.26
LO *Calcidiscus macintyrei*	1.67			6H-2, 140	6H-4, 110	49.10	51.80	50.45
LO *Discoaster brouweri*	1.95	NN19	CN14a-13a	6H-CC	7H-CC	56.12	65.71	60.92
LO *Discoaster surculus*	2.55	NN18-17	CN12d-c	8H-CC	9H-CC	74.34	84.56	79.45
LO *Discoaster tamalis*	2.83	NN16	CN12b-a	10H-CC	11H-CC	93.61	103.42	98.52
LO *Reticulofenestra pseudoumbilicus*	3.82	NN15	CN11	18H-CC	19H-CC	168.47	179.81	174.14
LO *Amaurolithus tricorniculatus*	4.5	NN14-13-12	CN10	20H-CC	21H-CC	188.61	198.67	193.64
LO *Discoaster quinqueramus*	5.54			22H-CC	23H-CC	206.71	213.47	210.09
				175-1087C-	175-1087C-			
LO *Amaurolithus amplificus*	5.9			27H-CC	28X-CC	248.58	258.40	253.49
FO *Amaurolithus amplificus*	6.6			30X-CC	31X-CC	270.96	280.46	275.71
FO *Amaurolithus primus*	7.2			33X-CC	34X-CC	299.68	309.35	304.52
FO *Discoaster quinqueramus*	8.6	NN11	CN9	41X-CC	42X-CC	375.29	386.21	380.75

Notes: FO = first occurrence and LO = last occurrence. Zonal codes are those from (A) Martini (1971) and (B) Okada and Bukry (1980).

and 31X-CC) was used to refine the age model of this interval. Sedimentation rate throughout this interval is ~ 5 cm/k.y.

Zone NN10

The Zone NN11/NN10 boundary was identified at Hole 1087C at the mean depth of 380.75 mbsf (FO of *D. quinqueramus;* 8.6 Ma).

Planktonic Foraminifers

Core-catcher samples from Holes 1087A and 1087C were analyzed. There is good general agreement between the planktonic foraminiferal and the calcareous nannofossil datums, despite the often very broad sampling interval that was used to identify datum levels.

Pleistocene

The late Pleistocene was identified by the absence of *Globorotalia tosaensis* (Table 3) at 13.2 mbsf. The presence of *G. tosaensis* and *G. truncatulinoides* (Samples 175-1087A-2H-CC through 4H-CC) define Zone Pl1a (13.2–41.6 mbsf).

Pliocene

The late Pliocene Zones Pl6–Pl3 (42–202 mbsf) were not differentiated because of the depauperate tropical fauna. The presence of *G. margaritae* (LO in Sample 175-1087A-22H-CC) marks the early Pliocene. Zones Pl2–Pl1b (202–210 mbsf) are undifferentiated, and Zone Pl1a (210–236 mbsf) is indicated by the presence of *G. margaritae* and *G. cibaoensis* in Samples 175-1087A-23H-CC and 24H-CC.

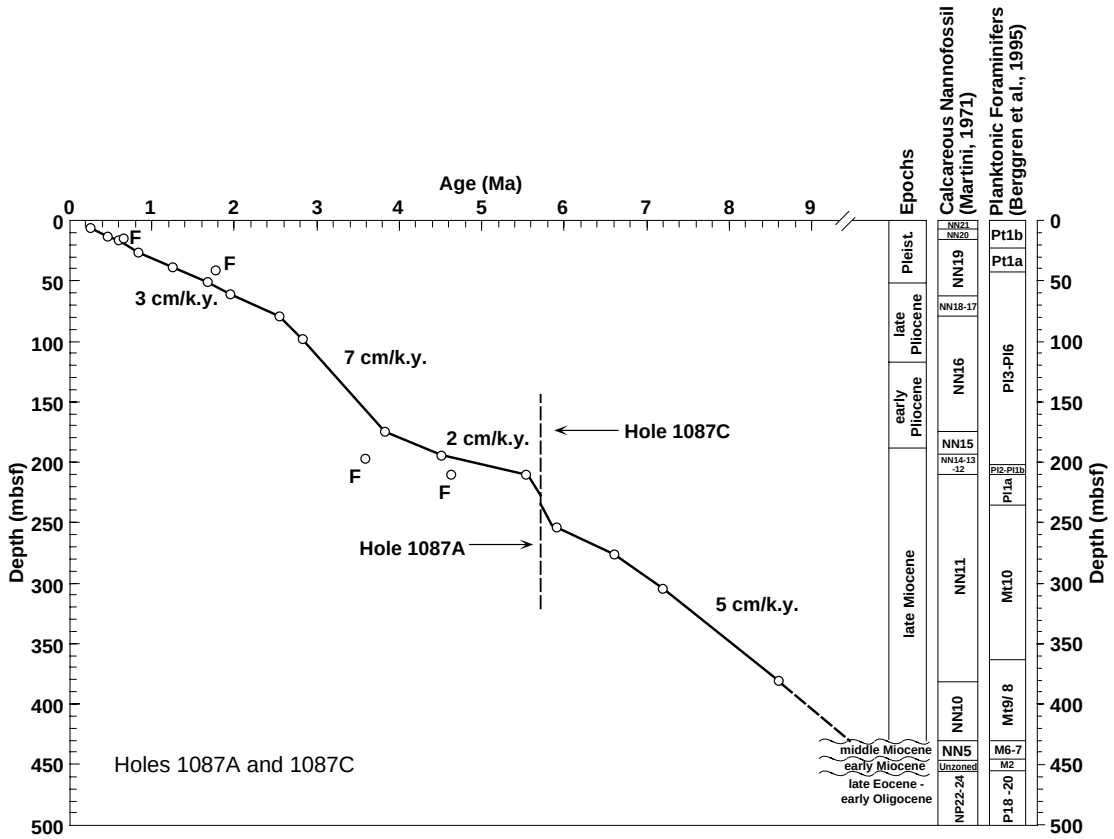

Figure 7. Age-depth plot and sedimentation rates estimated from calcareous microfossil (open circles; F = planktonic foraminifers and unlabeled = calcareous nannofossils) datums at Holes 1087A and 1087C.

Table 3. Planktonic foraminiferal datums at Holes 1087A and 1087C.

Event	Age (Ma)	Zone	Core, section, interval (cm) Top	Core, section, interval (cm) Bottom	Depth (mbsf) Top	Depth (mbsf) Bottom	Depth (mbsf) Mean
			175-1087A-	175-1087A-			
LO *Globorotalia tosaensis*	0.65	Pt1b bottom	1H-CC	2H-CC	8.21	18.17	13.19
FO *Globorotalia truncatulinoides*	1.77	Pt1a bottom	4H-CC	5H-CC	36.71	46.55	41.63
LO *Globorotalia margaritae*	3.58	Pl2 top	21H-CC	22H-CC	198.67	206.71	202.69
LO *Globorotalia cibaoensis*	4.6	Pl1a top	22H-CC	23H-CC	206.71	213.47	210.09
FO *Globorotalia sphericomiozea*	5.6		24H-CC	25H-CC	227.18	236.17	231.68
			175-1087C-	175-1087C-			
FO *Globorotalia conomiozea*	6.9	MT10 bottom	29H-CC	30H-CC	262.4	270.96	266.68
FO *Globorotalia nepenthes*	11.8	MT8 bottom	46H-CC	47H-CC	424.79	433.09	428.94

Note: FO = first occurrence and LO = last occurrence.

Miocene

Faunas restricted to late Miocene Zone Mt10 are found in Samples 175-1087A-26H-CC, 175-1087C-29X-CC, and 175-1087C-39X-CC (236–361 mbsf). Zones Mt9 and Mt8 (361–429 mbsf) are undifferentiated. The late Miocene is separated from the middle Miocene by an unconformity between Samples 175-1087C-46X-CC and 47X-CC. This biostratigraphic break is correlative with a sharp lithologic break in the core (see "Lithostratigraphy" section, this chapter). Samples 47X-CC and 48X-CC contain fauna from middle Miocene Zones M6–M7 (429–447 mbsf). There is probably another unconformity between Samples 48X-CC and 49X-CC, because the faunas in Sample 49X-CC are restricted to early Miocene Zone M2 and older. The age estimate is uncertain, however, because reworking occurs in this interval (447–454 mbsf).

Eocene and Oligocene

Samples 175-1087C-50H-CC through 53H-CC contain fauna restricted to the late Eocene to early Oligocene. There is a significant unconformity between the lower Miocene (Sample 175-1087C-49X-CC) and the upper Eocene/lower Oligocene (Sample 50X-CC) sequences.

Benthic Foraminifers

The benthic foraminiferal fauna of Site 1087 was studied in the core-catcher samples from Hole 1087A. The benthic foraminifers are abundant throughout Hole 1087A, but as at previous sites in the Cape Basin (Sites 1085 and 1086), there is a very high planktonic to benthic foraminifer ratio. The preservation of the benthic foraminiferal assemblage is good throughout Hole 1087A.

The uppermost core catcher (Sample 175-1087A-1H-CC; 8.21 mbsf) is dominated by *Bulimina aculeata*, together with *Uvigerina hispidocostata* (Table 4).

The Pleistocene and the late Pliocene (down to ~160 mbsf) are dominated by *Bulimina mexicana, Hoeglundina elegans*, and stilostomellas (Table 4). *Uvigerina peregina* is an important component of the fauna in the lowermost Pleistocene and uppermost upper Pliocene sequences. The lowermost upper Pliocene sediment contains *Siphotextularia concava.*

The lower Pliocene and uppermost upper Miocene sediments recovered from Hole 1087A are strongly dominated by *Bolivina subaenarensis*, together with *Bulimina mexicana*, *Cibicidoides pachyderma, Ehrenbergina trigona,* and *Uvigerina auberiana* (Table 4). The lowermost core catcher (Sample 175-1087A-27H-CC; 255.15 mbsf) contains a high abundance of *Bolivina pseudoplicata* (Table 4).

Radiolarians

Core-catcher samples from Cores 175-1087A-1H-CC through 27H-CC and 1087C-27H-CC through 39X-CC, 42X-CC, 44X-CC, 46X-CC, 48X-CC, 50X-CC, 52X-CC, and 53X-CC were examined for radiolarians (Table 5). At Hole 1087A, radiolarians are generally rare and show signs of dissolution. Samples 175-1087A-17H-CC through 27H-CC are barren of radiolarians. No radiolarians could be identified from the examined samples from Hole 1087C.

The absence of *Axoprunum angelinum* indicates that the uppermost samples (175-1087A-1H-CC and 2H-CC) belong to Zone NR1 of Caulet (1991). It was not possible to determine a zone for samples below Sample 2H-CC because of the scarcity or absence of age-diagnostic taxa. The LO of *Lamprocyrtis neoheteroporos* in Sample 175-1087A-4H-CC probably indicates an age of 1.07 Ma. The FO of *Cycladophora davisiana* indicates an age of 2.70 Ma for Sample 175-1087A-9H-CC.

The *Axoprunum stauraxonium* and *Ellipsoxiphus attractus* groups are common in Samples 175-1087A-1H-CC, 2H-CC, 5H-CC, 6H-CC, 12H-CC, 13H-CC, 14H-CC, 15H-CC, and 16X-CC, indicating low productivity under subtropical warm-water conditions. The radiolarian assemblages that are characterized by common *C. davisiana* suggest upwelling conditions for Samples 175-1087A-7H-CC and 8H-CC. The presence of an Antarctic species, *Cycladophora pliocenica,* in Sample 175-1087A-12H-CC indicates an influence of cooler water.

Diatoms

Core-catcher samples from Holes 1087A (1H-CC through 27H-CC) and 1087C (27H-CC through 53X-CC) were analyzed for their diatom content. Samples were acid-cleaned, rinsed in distilled water, and sieved through a 20- or 63-µm sieve before smear slides were prepared. Diatoms are present (rare to few) in the upper Pliocene sediment only, between Samples 175-1087A-7H-CC (65.71 mbsf) and 13H-CC (122.85 mbsf). As at Site 1085, this interval includes a mixed *Thalassiothrix antarctica*–rich assemblage (composed of Southern Ocean species and warm oceanic species), with an approximate age of 1.9–2.8 Ma. Diatoms are barren below 122 mbsf at Hole 1087A and in the analyzed portion of Hole 1087C.

Sponge spicules are present only in the Pleistocene and upper Pliocene sediments (from Samples 175-1087A-1H-CC through 18H-CC; 8.21 to 168.44 mbsf); they are particularly abundant in the Pleistocene. Dinoflagellate cysts are common below 213 mbsf (Sample 23H-CC) at Hole 1087A, and between 262 (Sample 29X-CC) and 338 mbsf (37X-CC) at Hole 1087C. The age of the LO of dinoflagellate cysts at Hole 1087A approximates that of Sites 1085 and 1086 (~5.8 Ma), suggesting that both sites were affected by the same oceanographic process simultaneously.

PALEOMAGNETISM

The investigation of magnetic properties at Site 1087 included the measurement of magnetic susceptibility of whole-core sections and the natural remanent magnetization (NRM) of archive-half sections. The Tensor tool was used to orient Cores 175-1087A-3H through 27H (except for 17H), 175-1087B-3H through 8H, 175-1087C-4H through 27H (except for 20H), and 175-1087D-1H through 11H (Table 6).

Natural Remanent Magnetization, Magnetic Susceptibility, and Magnetic Overprint

Measurements of NRM were made on all archive-half core sections from Holes 1087A, 1087B, 1087C, and 1087D. All sections were demagnetized by AF at 20 mT. Magnetic susceptibility measurements were made on whole cores from all holes, except 1087D, as part of the MST analysis (see "Physical Properties" section, this chapter).

The intensity of NRM after 20-mT demagnetization is between ~10^{-3} and 10^{-5} A/m, except for below 432 mbsf at Hole 1087C, where the intensity is ~10^{-2} A/m. Magnetic susceptibility ranges between 0 and 5×10^{-5} (SI volume units) for the upper 432 mbsf and between 10 and 20×10^{-5} below 432 mbsf. The trends in variations in remanent intensity and magnetic susceptibility are not parallel, except for the sudden increase below 432 mbsf.

APC suffered significant coring-induced magnetization (CIM) with a radial-inward direction (see "Paleomagnetism" sections, "Site 1077" and "Site 1081" chapters, this volume). The CIM is evident from the clustering of declinations around 0° before orientation. In contrast, inclinations showed distinct polarity biases after 20-mT demagnetization, from which an interpretation of the magnetic polarity

Table 4. Relative abundance of benthic foraminiferal species and overall abundance of benthic foraminifers at Hole 1087A.

Core, section, interval	Depth (mbsf)	Abundance	*Anomalinoides globulosus*	*Astrononion novozealandicum*	*Astrononion stelligerum*	*Bolivina pseudoplicata*	*Bolivina subaenarensis*	*Bolivina seminuda*	*Bolivinopsis cubensis*	*Bulimina aculeata*	*Bulimina mexicana*	*Bulimina truncana*	*Cassidulina laevigata*	*Cassidulina minuta*	*Cassidulinoides* cf. *bradyi*	*Chilostomella ovoidea*	*Cibicidoides bradyi*	*Cibicidoides pachyderma*	*Cibicidoides wuellerstorfi*	*Cibicidoides* sp. 1	*Dorothia* cf. *brevis*	*Eggerella bradyi*
175-1087A-																						
1H-CC	8.21	A								21	5					+		5				+
3H-CC	27.75	A			+					2	11		9		2			3	5			
5H-CC	46.55	A									+		11				+	7	+			1
7H-CC	65.71	A			+			+			10					1		+	2			+
9H-CC	84.56	A									8						6		+			2
11H-CC	103.42	A						+			4				+				7			
13H-CC	122.85	A		1							3			1			2		3			2
15H-CC	141.72	A									15				+				3			
17H-CC	159.54	A	+								7						+	6	2	2	+	1
19X-CC	179.81	A					26				8						1	3	4			1
21X-CC	198.67	A					27				7	+			+		2	7	+			6
23X-CC	213.47	A	7				5				2						2	13	6	+		1
25X-CC	236.17	A	2			+	4				13			+			4	17	4			+
27X-CC	255.15	A				12	22		+		4					+	4	7	+	+		1

Core, section, interval	*Ehrenbergina pupa*	*Ehrenbergina trigona*	*Epistominella exigua*	*Fissurina* spp.	*Fursenkoina* sp. 1	*Gavelinopsis lobatulus*	*Globocassidulina subglobosa*	*Gyroidinoides soldanii*	*Hoeglundina elegans*	*Karreriella bradyi*	*Laticarinina pauperata*	*Martinottiella communis*	*Melonis barleeanum*	*Oolina* spp.	*Oridorsalis umbonatus*	*Plectofrondicularia* cf. *inaequalis*	*Plectofrondicularia* cf. *raricosta*	*Plectofrondicularia* cf. *semicosta*	*Pleurostomella alternans*	*Praeglobobulimina/Globobulimina* group
175-1087A-																				
1H-CC			1	+	+		+	1	+	+		+			+					2
3H-CC			2		2		2								13	+	2			13
5H-CC							2	2							2					1
7H-CC				+	+		4		6	+					6	+	+			+
9H-CC			3	+	+	2			7	1		+	3		4		+			1
11H-CC			1			4			16				7	+	7	2				+
13H-CC			3	+		2	+		27		+	+	+		+				+	1
15H-CC			11	+					3				7		7		+			
17H-CC			5	+		+		1	7	+		+	1		4	+	1	+	+	1
19X-CC			+	+			4	2	7		+		4		2	+			+	
21X-CC	+	1		+		+							2		3				+	1
23X-CC		4	+				2	2		4	+		1		4					+
25X-CC	1	11	4	+				+		+	1	1	3		5	+	+			+
27X-CC	+	+	3	+			8				+	+	2		8				+	

Core, section, interval	*Pullenia bulloides*	*Pullenia subcarinata*	*Pyrgo* spp.	*Quadrimorphina allomorphinoides*	*Sigmoilinopsis schlumbergeri*	*Sigmoilinita* sp. 1	*Siphotextularia catenata*	*Siphotextularia concava*	*Siphotextularia rolshauseni*	*Sphaeroidina bulloides*	*Stilostomella* spp.	*Trifarina angulosa*	*Trifarina bradyi*	*Uvigerina auberiana*	*Uvigerina gallowayi*	*Uvigerina hispida*	*Uvigerina hispidocostata*	*Uvigerina peregrina*	Unidentified	Number of specimens counted
175-1087A-																				
1H-CC		+	7	+				2		7						+	38	1	2	310
3H-CC	2		7	+	3			5		3	+			+		+	5		5	128
5H-CC	+	+	1			1				+	7		3	2		+	35	11	8	285
7H-CC		+	3	+	11					+	11			2			3	22	12	235
9H-CC	1	1	2	+						2	4			4			2	27	15	222
11H-CC	4	+	1	2						4	6			23			1	+	7	227
13H-CC	4	+	1		2	+		14		10	6			6			3		4	232
15H-CC	4	+		1				5			15	+		2			20	+	3	301
17H-CC	2	+	1	1	+			9		6	5			7			17		8	350
19X-CC	+		3		1			6		4	4			9			+		9	269
21X-CC	+	+	3	1	2				+	+	5			12			7		8	273
23X-CC	2		3		5			+		7	1		+	12		2	2		9	307
25X-CC	2	+	1	+	1	+		+		+				2	+	1	9		6	254
27X-CC	3		3	+			+		1	1	5			+		3			6	267

Notes: The relative abundance of benthic foraminiferal species is given as a percentage, where + = <1% and P = present (the relative abundance was not calculated because of small sample size). Absolute abundance (per ~20 cm^3 of sediment) of benthic foraminifers is given as A = abundant (>500 specimens).

Table 5. Stratigraphic distribution of radiolarians at Hole 1087A.

Core, section, interval	Depth (mbsf)	Abundance	Preservation	*Cycladophora davisiana*	*Didymocyrtis tetrathalamus*	*Pterocanium trilobum*	*Axoprunum angelinum*	*Lamprocyclas hannai*	*Pterocanium praetextum eucolpum*	*Spongurus pylomaticus*	*Theocorythium trachelium*	*Eucyrtidium calvertense*	*Lamprocyrtis neoheteroporos*	*Lamprocyrtis heteroporos*	*Amphirhopalum ypsilon*	*Eucyrtidium teuscheri*	*Didymocyrtis avita*	*Eucyrtidium acuminatum*	*Cycladophora cornutoides*	*Cycladophora sakaii*	*Cycladophora pliocenica*
175-1087A-																					
1H-CC	8.21	C	M	P	P	+															
2H-CC	18.17	R	M																		
3H-CC	27.75	A	M	P	P		P	P	+	+	P										
4H-CC	36.71	A	M	P	P		P	P				+	P								
5H-CC	46.55	A	M	P	P		+					P		+							
6H-CC	56.12	A	M	P	P			+				P									
7H-CC	65.71	A	M	P	P	P		P		+	P	P	+		+	+					
8H-CC	74.34	A	M	P	P	+		P				P			P		P				
9H-CC	84.56	A	M	P	P		P	P	+			P		P	+			+			
10H-CC	93.61	A	M		P	+	P	+			P	P	+	P	P	+	P	P	P	+	
11H-CC	103.42	A	M		+		P	+				P	+	P							
12H-CC	112.97	A	M		P		P	P				P	+	P		+	P				+
13H-CC	122.85	A	M					P				+									
14H-CC	131.80	R	P																		
15H-CC	141.72	F	M																		
16H-CC	150.83	R	M																		
17H-CC	159.54	B																			
18H-CC	168.44	B																			
19H-CC	179.81	B																			
20H-CC	188.61	B																			
21H-CC	198.67	B																			
22H-CC	206.71	B																			
23H-CC	213.47	B																			
24H-CC	227.18	B																			
25H-CC	236.17	B																			
26H-CC	242.12	B																			

Notes: Occurrence is indicated by P = present and + = one specimen per slide. Abundance: C = common; R = rare; A = abundant; F = few; and B = barren. Preservation: M = moderate and P = poor.

was possible. However, the uppermost parts of many cores showed anomalous steep negative inclinations, even after the data from physically disturbed sediments were discarded. One explanation is that some of the disturbance was not physically apparent.

XCB cores from Hole 1087C between 250 and 400 mbsf show extremely strong scatter in both declinations and inclinations, and we could not identify the polarity of NRM (Fig. 8C). However, biases in inclination possibly caused by polarity reversals can be recognized. XCB cores below 400 mbsf show a clustering of declinations around 0°, which indicates a radial-inward magnetic overprint. The direction is different from the nonaxisymmetric declination of –20° to –30° observed in XCB cores of previous sites (see "Paleomagnetism" sections, "Site 1081," "Site 1082," "Site 1084," and "Site 1085" chapters, this volume). Inclinations below 400 mbsf are biased toward positive polarity.

Magnetostratigraphy

We identified the polarity of the NRM mainly from the inclinations (Fig. 8) of APC cores from Holes 1087A and 1087C. Further study of all holes drilled at this site may clarify the preliminary interpretations presented here. Considering constraints from the biostratigraphy (see "Biostratigraphy and Sedimentation Rates" section, this chapter), we interpreted the polarity reversal sequence from Chrons C1n to C2Ar (~ 4 Ma). Magnetostratigraphic interpretation is summarized in Table 7 using the time scale of Berggren et al. (1995).

Interpretation of the Brunhes/Matuyama boundary was problematic. Two possible interpretations are presented in Figure 8. If the upper limit for the Brunhes/Matuyama boundary is used (27 mbsf; Table 7), then the Jaramillo event may be responsible for the anomalous directions between 27 and 39 mbsf. The Jaramillo, therefore, is only tentatively interpreted in Figure 8 and Table 7, based on the lower limit for the Brunhes/Matuyama boundary (39 mbsf; Table 7). The biostratigraphy suggests that turbidites may be present within the upper ~60 mbsf (see "Biostratigraphy and Sedimentation Rates" section, this chapter), which may account for the disagreement between

Table 6. Tensor tool–orientation data for cores from Holes 1087A, 1087B, 1087C, and 1087D.

Core	MTF (°)	Inclination angle
175-1087A-		
3H	350	0.65
4H	315	0.55
5H	82	0.58
6H	30	0.38
7H	309	0.78
8H	299	0.21
9H	335	0.35
10H	14	0.47
11H	236	0.28
12H	288	0.39
13H	288	0.69
14H	151	0.42
15H	147	0.80
16H	74	0.62
18H	134	0.75
19H	92	0.64
20H	213	0.93
21H	344	0.98
22H	253	1.04
23H	244	0.97
24H	22	0.76
25H	88	0.87
26H	262	1.04
27H	287	0.97
175-1087B-		
3H	148	0.78
4H	119	0.64
5H	90	0.92
6H	0.73	0.84
7H	185	0.83
8H	234	0.76
175-1087C-		
4H	45	0.45
5H	14	0.48
6H	47	0.49
7H	344	0.50
8H	42	0.40
9H	137	0.42
10H	174	0.54
11H	88	0.66
12H	65	0.49
13H	311	0.48
14H	334	0.57
15H	352	0.45
16H	48	0.62
17H	42	0.49
18H	90	0.46
19H	226	0.51
21H	219	0.45
22H	276	0.50
23H	31	0.95
24H	112	1.08
25H	90	1.28
26H	152	1.29
27H	117	1.36
175-1087D-		
1H	3	0.45
2H	95	0.50
3H	161	0.83
4H	81	0.56
5H	180	0.52
6H	43	0.64
7H	87	0.35
8H	307	0.77
9H	58	0.26
10H	284	0.62
11H	267	0.78

Notes: The orientation parameter (MTF) is the angle in degrees between magnetic north and the double line marked on the center of the working half of the core. The local declination anomaly is 21°W.

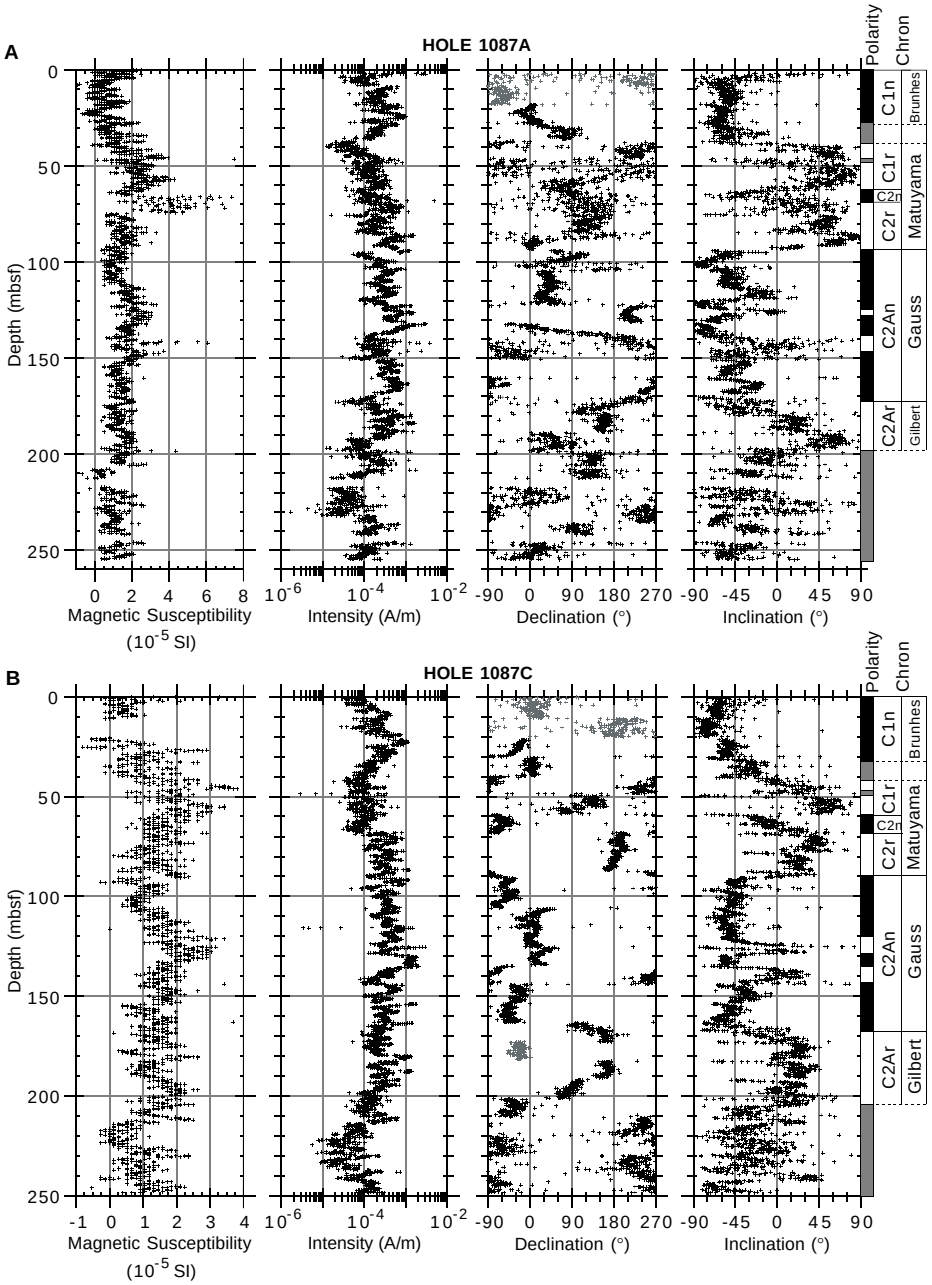

Figure 8. Magnetic susceptibility (SI volume units) and NRM intensity, declination, inclination, and magnetostratigraphic interpretation after 20-mT demagnetization. Black symbols = Tensor corrected; gray symbols = uncorrected. Polarity shading: black = normal, white = reversed, and gray = ambiguous. **A.** Hole 1087A. **B.** Hole 1087C (APC cores only). (Continued on next page.)

the magnetostratigraphy and the biostratigraphic interpretations within this interval. Between ~60 and 200 mbsf, the magnetostratigraphic interpretation agrees well with the biostratigraphy. Between about 200 and 250 mbsf, however, the inclinations are highly scattered and the declinations are clustered around 0° before orientation, which precluded polarity interpretation.

COMPOSITE SECTION

At Site 1087, four holes were cored with a maximum penetration of 491.9 mbsf. Physical properties data were measured at 5-cm (Hole 1087A, 0–60 mbsf) and 10-cm (Hole 1087A [below 60 mbsf] and Holes 1087B and 1087C) intervals. Physical properties for Hole 1087D were not measured. The correlation of features present in the physical properties measurements of adjacent holes was used to demonstrate the completeness of the local stratigraphic sequence drilled and to establish a depth scale in terms of meters composite depth (mcd) for Site 1087. The continuity of the stratigraphic sequence could be demonstrated between 0 and 214 mcd (Figs. 9, 10; Table 8).

At Site 1087, magnetic susceptibility and GRAPE density were used to establish the mcd scale. The data sets were extensively processed before being used for correlation. Suspect measurements were eliminated by thresholding the data. The resulting data were

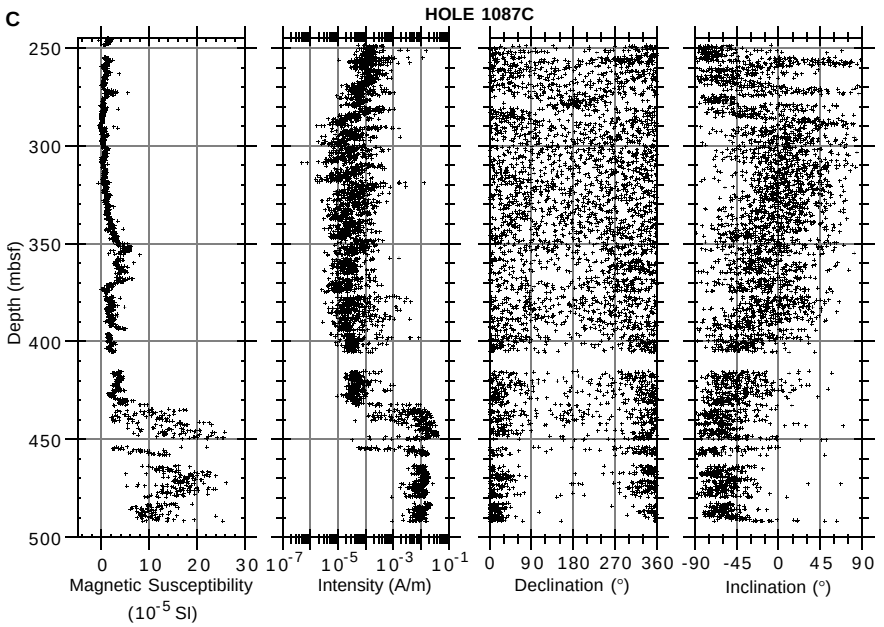

Figure 8 (continued). **C**. Hole 1087C (XCB cores only).

Table 7. Magnetostratigraphic interpretations for Site 1087.

Polarity chron	Age (Ma)	Depth (mbsf) Hole 1087A	Depth (mbsf) Hole 1087C	Polarity epoch
C1n/C1r.1r	0.78	27-39	32-43	Brunhes/Matuyama
C1r.1n	0.99-1.07	46-48	47-49	Jaramillo(?)
C2n	1.77-1.95	63-68	59-68	Olduvai
C2An.1n (top)	2.58	93	90	Gauss
C2An.1r (bottom)	3.11	128	129	Kaena
C2An.2r (bottom)	3.33	147	143	Mammoth
C2Ar (top)	3.58	173	168	Gilbert

Note: Time scale used is that of Berggren et al. (1995).

smoothed using a 31-cm Gaussian filter. All data shown in Figures 9 and 10 were processed as described above.

The spliced record presented in Figure 10 is continuous to 214 mcd for magnetic susceptibility and wet bulk density (Table 9). The selection of cores to be included in the spliced record and the placement of tie points were carried out mainly using the composite section of magnetic susceptibility.

The growth of the mcd scale compared with the standard ODP mbsf scale is ~10% (Core 175-1087B-21H at 205 mcd and 182 mbsf; Fig. 11).

INORGANIC GEOCHEMISTRY

Because of time constraints at the end of the leg, samples were gathered only from Hole 1087A between 1.4 and 201.1 mbsf and from Hole 1087C between 224.5 mbsf to total depth. Whole-round samples were sampled at a frequency of one sample per core to 98.1 mbsf and every third core thereafter to 477.45 mbsf (Table 10). Only the samples from Hole 1087A were analyzed for properties other than salinity, pH, and alkalinity. Shore-based efforts will complete these traditionally shipboard analysis for Hole 1087C. Compared with the other Leg 175 Cape Basin drill sites, the chemical gradients observed at Site 1087 are intermediate between those at Sites 1085 and 1086, yet more similar to those at Site 1085.

Alkalinity, Sulfate, and Ammonium

Downcore profiles of alkalinity, sulfate, and ammonium (Fig. 12) reflect the degradation of organic matter. Alkalinity reaches a maximum value of 31 mM at 79 mbsf and subsequently decreases to a minimum value of 2.134 mM to the bottom of Hole 1087C. The deeper decrease likely is largely caused by alkalinity consumption during clay mineral formation ("reverse weathering"; see Mg^{2+} below). Sulfate is completely consumed by 79 mbsf, which is intermediate in depth between the depth of sulfate consumption observed at Sites 1085 and 1086. Ammonium reaches a maximum value of only ~4900 µM at 155 mbsf before starting to decrease with depth.

Calcium and Magnesium

From the seafloor to 89 mbsf, the concentrations of dissolved Ca^{2+} and Mg^{2+} decrease sharply. The decrease in Ca^{2+} through this depth range (6 mM) is significantly less than the decrease in dissolved Mg^{2+} (13 mM). This lack of correspondence in both extent and pattern of these respective decreases suggests that dolomitization is not an important process at this site. Rather, we attribute the decrease in Ca^{2+} mainly to phosphate precipitation and the decrease in Mg^{2+} mainly to clay mineral uptake.

From 89 mbsf to the bottom of Hole 1087A, concentrations of dissolved Ca^{2+} increase smoothly, with the possible exception of the interval from ~98 to 212 mbsf, where there appears to be a positive excursion above the general trend of the increase (see shaded portion of Fig. 13). Through this same interval, dissolved Mg^{2+} concentrations may also be slightly above the overall decreasing trend. Regardless of these excursions, the broad increase in dissolved Ca^{2+} most likely reflects dissolution of biogenic calcite, whereas the decrease in Mg^{2+} reflects uptake by clay minerals.

Silica and Phosphate

Dissolved silica is present in interstitial waters from Site 1087 at concentrations greater than representative bottom-water values (Fig. 14), indicating dissolution of biogenic opal. There appear to be three depth domains of dissolved silica distribution. The first, from the seafloor to 22 mbsf, describes the greatest increase in dissolved silica. From this depth to 60 mbsf, dissolved silica concentrations remain essentially constant at ~ 615 µM. Following a rapid rise to a maximum of 714 µM at 79 mbsf, dissolved silica concentrations decrease with depth to the bottom of Hole 1087A. The decrease most likely records clay mineral uptake.

Dissolved phosphate concentrations increase with depth to reach a maximum of 50–70 µM from 60 to 70 mbsf (Fig. 14). Excluding the

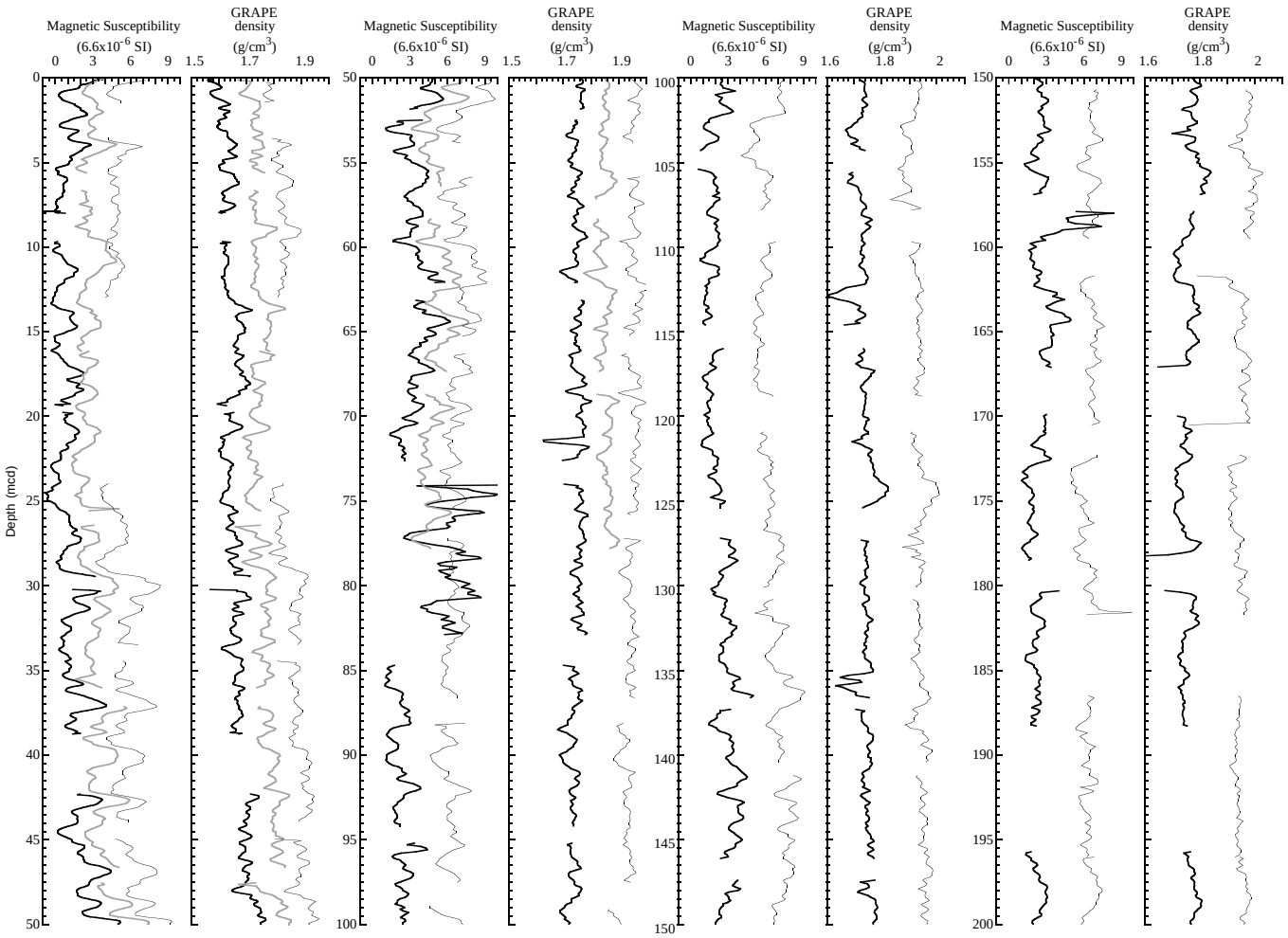

Figure 9. Composite section for Site 1087. Magnetic susceptibility and wet bulk density (GRAPE) are plotted for Holes 1087A (thick black line), 1087B (gray line), and 1087C (thin black line). The downhole logs are shown in meters composite depth (mcd). Offsets have been applied for clarity.

one point off the trend, the maximum itself is very broad and diffuse, and toward the deeper portion of the sequence dissolved phosphate concentrations decrease to values of ~10 µM, thereby recording uptake of dissolved phosphate into authigenic phases.

Sodium and Potassium

Dissolved Na^+ increases rapidly through the uppermost 88 mbsf and decreases to 155 mbsf before increasing to the bottom of Hole 1087A (Fig. 15). Concentrations of dissolved K^+ decrease to the bottom of the hole. There is a one-point maximum in dissolved K^+ at 31.6 mbsf that corresponds with a one-point minimum in dissolved Na^+; as discussed below, this may also be recorded in the salinity profile.

Salinity and Chloride

Salinity shows a general decrease from 35.0 to 32.5 through the sequence (Fig. 16) but records a strong increase to a maximum value of 37.5 at 50.6 mbsf. This maximum is not defined by a single point; rather, there is a marked increase in salinity from 22 mbsf to this maximum at 50.6 mbsf. This depth range includes the depth at which the one-point maximum in dissolved K^+ is observed, suggesting that some—at this point unknown—reactions are occurring to simultaneously affect these chemical profiles. Concentrations of dissolved (Cl^-) record an initial increase to a maximum of ~560 mM at 31.60 mbsf before decreasing to 547 mM at 126 mbsf. Below this depth, dissolved Cl^- remains essentially constant to the bottom of Hole 1087A. The initial increase in dissolved Cl^- may reflect changes in bottom-water chemistry associated with ice-volume variations through glacial periods. With the exception of the salinity variation in the uppermost sediment, both the salinity and Cl– profiles are very similar to those observed at Sites 1085 and 1086.

ORGANIC GEOCHEMISTRY

Because of time limitations between coring and entering port, the only organic geochemical measurements that were performed entailed routine monitoring of the sedimentary gases for drilling safety.

Headspace Gases

Moderately high amounts of methane and CO_2 were found in sediments from Site 1087 (Table 11). The odor of hydrogen sulfide was noted in cores from 5 to 250 mbsf. Total gas pressures became great enough in sediments between 15 and 200 mbsf to require perforating the core liner to relieve the pressure and prevent excessive core expansion.

Methane (C_1) first appears in headspace gas samples from Site 1087 sediments at 22.2 mbsf. Concentrations become significant in sediments below 60 mbsf (Fig. 17). The rate of methane appearance is slower than in most sites cored during Leg 175. High methane/ethane (C_1/C_2) ratios and the absence of major contributions of higher

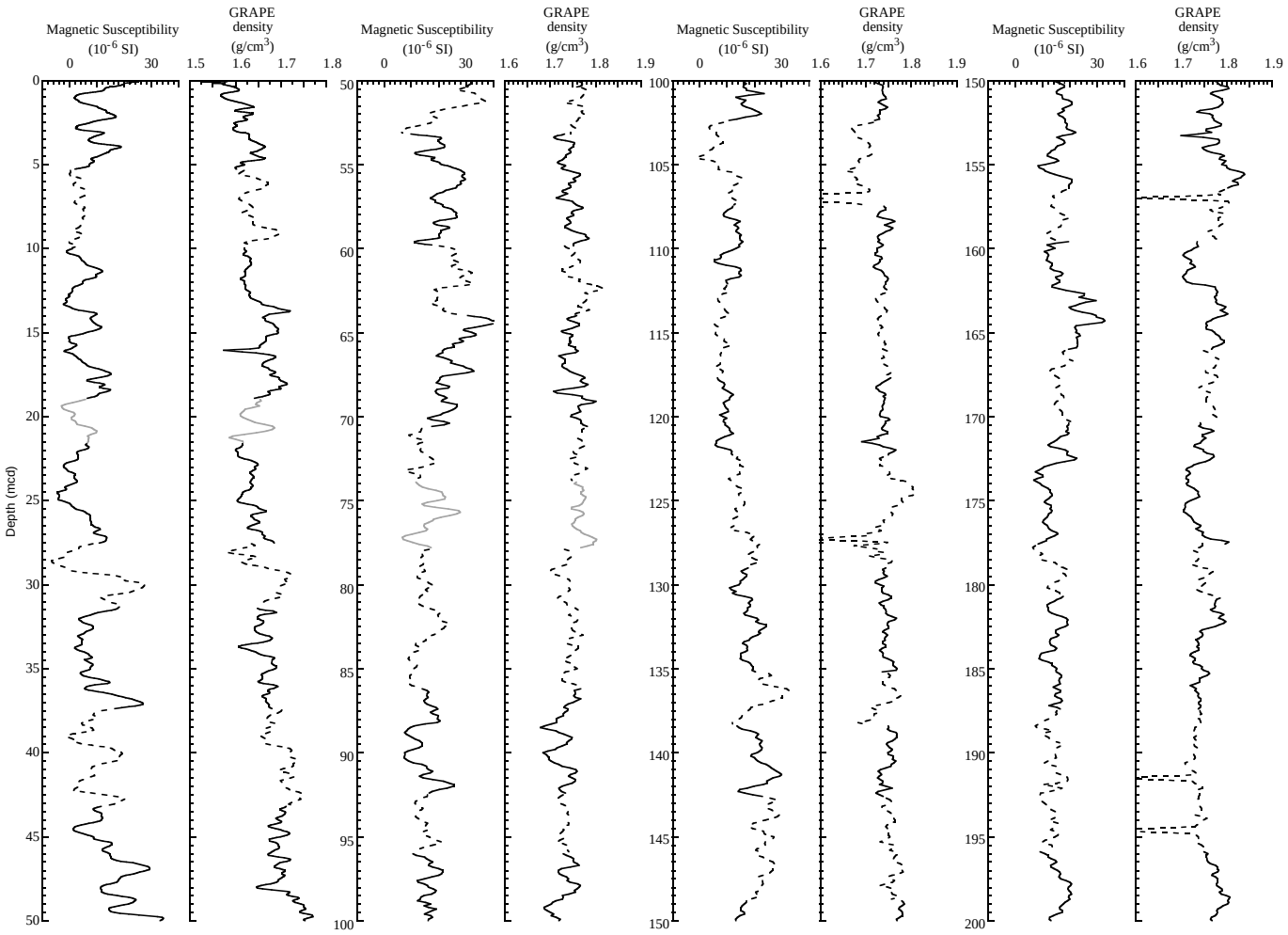

Figure 10. Spliced records for magnetic susceptibility and wet bulk density (GRAPE) plotted in meters composite depth (mcd). Cores from Holes 1087A, 1087B, and 1087C have been used for the spliced record: solid black line = Hole 1087A, gray line = Hole 1087B, and dashed line = Hole 1087C.

molecular weight hydrocarbon gases (Table 11) indicate that the gas is biogenic, as opposed to thermogenic, in origin. As at Sites 1084 through 1086, the origin of the methane is probably from in situ microbial fermentation of the marine organic matter present in the sediments. A biogenic origin of methane is supported by the disappearance of interstitial sulfate at approximately the same sub-bottom depth where methane concentrations begin to rise (see "Inorganic Geochemistry" section, this chapter), inasmuch as Claypool and Kvenvolden (1983) observe that the presence of interstitial sulfate inhibits microbial methanogenesis in marine sediments.

The most abundant gas is CO_2 in the upper 350 m of Hole 1087C. Concentrations of this gas decrease sharply below this depth (Fig. 18). Methane concentrations gradually increase downhole until methane dominates gas compositions in sediments deeper than 350 mbsf, even though methane concentrations never equal those of shallower CO_2 concentrations (Table 11). Cragg et al. (1992) report the existence of viable microbes to depths of ~500 mbsf in the sediments of the Japan Sea. The abundance of biogenic gases deep in sediments at Site 1087 suggests the presence of viable microbial communities to similar sub-bottom depths on the southwest African margin.

PHYSICAL PROPERTIES

A minimum program of shipboard physical properties measurements was carried out at Site 1087. Measurements with the MST were conducted at a 10-cm resolution for GRAPE wet bulk density, magnetic susceptibility, and *P*-wave velocity on all recovered whole-round core sections.

Gravimetric wet bulk density, porosity, and moisture content data were determined from one sample point in every half-split core section. Method C was used at Site 1087 (see "Explanatory Notes" chapter, this volume).

Discrete compressional (*P*-wave) velocity measurements were made at a resolution of one sampling point per section. For these *P*-wave velocity measurements, the modified Hamilton Frame was used on split-core sections between 0 and 255 mbsf.

Thermal conductivity was determined on every fifth unsplit section in every core by inserting a thermal probe into the sediment (see "Explanatory Notes" chapter, this volume).

Multisensor Track

GRAPE density (Fig. 19), *P*-wave velocity (Fig. 20), and magnetic susceptibility (Fig. 21A) were recorded every 10 cm for the entire depth at Hole 1087A. MST data are included on CD-ROM (back pocket, this volume). Compressional velocities were stored at an amplitude threshold of 50 incremental units. The MST *P*-wave logger recorded signals over the entire depth range of 255 mbsf at Hole 1087A (Fig. 20), which correlate well with discrete velocities. Discrete velocities were generally higher (Fig. 20), although MST velocities are higher between 170 and 205 mbsf.

Magnetic susceptibility (Fig. 21A) shows a trend similar to that of GRAPE density and index properties wet bulk density (Figs. 19,

Table 8. Offsets applied to cores from Holes 1087A, 1087B, and 1087C.

Core	Depth (mbsf)	Offset (m)	Composite depth (mcd)
175-1087A-			
1H	0.0	0.00	0.00
2H	8.2	1.37	9.57
3H	17.7	1.97	19.67
4H	27.2	2.92	30.12
5H	36.7	5.50	42.20
6H	46.2	6.20	52.40
7H	55.7	7.35	63.05
8H	65.2	8.65	73.85
9H	74.7	9.85	84.55
10H	84.2	10.85	95.05
11H	93.7	11.55	105.25
12H	103.2	12.65	115.85
13H	112.7	14.35	127.05
14H	122.2	14.95	137.15
15H	131.7	15.55	147.25
16H	141.2	16.55	157.75
17H	150.7	19.04	169.74
18H	160.2	19.95	180.15
19H	169.7	25.85	195.55
20H	179.2	26.15	205.35
21H	188.7	31.05	219.75
22H	198.2	31.15	229.35
23H	207.7	31.15	238.85
24H	217.2	31.15	248.35
25H	226.7	31.15	257.85
26H	236.2	31.15	267.35
27H	245.7	31.15	276.85
175-1087B-			
1H	0.0	–0.12	–0.12
2H	6.0	0.52	6.52
3H	15.5	0.52	16.02
4H	25.0	1.27	26.27
5H	34.5	2.50	37.00
6H	44.0	3.40	47.40
7H	53.5	4.70	58.20
8H	63.0	5.55	68.55
175-1087C-			
1H	0.0	0.00	0.00
2H	1.6	1.82	3.42
3H	11.1	3.22	14.32
4H	20.6	4.20	24.80
5H	30.1	5.20	35.30
6H	39.6	6.60	46.20
7H	49.1	7.55	56.65
8H	58.6	8.95	67.55
9H	68.1	10.35	78.45
10H	77.6	11.65	89.25
11H	87.1	12.95	100.05
12H	96.6	14.65	111.25
13H	106.1	15.05	121.15
14H	115.6	15.95	131.55
15H	125.1	15.95	141.05
16H	134.6	17.44	152.04
17H	144.1	18.53	162.63
18H	153.6	23.25	176.85
19H	163.1	23.25	186.35
20H	172.6	23.15	195.75
21H	182.1	23.15	205.25
22H	191.6	23.15	214.75
23H	201.1	23.15	224.25
24H	210.6	23.15	233.75
25H	220.1	23.15	243.25
26H	229.6	23.15	252.75
27H	239.1	23.15	262.25
28X	248.6	23.15	271.75
29X	254.9	23.15	278.05
30X	261.2	23.15	284.35
31X	270.8	23.15	293.95
32X	280.4	23.15	303.55
33X	290.0	23.15	313.15
34X	299.7	23.15	322.85
35X	309.3	23.15	332.45
36X	318.9	23.15	342.05
37X	328.5	23.15	351.65
38X	338.2	23.15	361.35
39X	347.8	23.15	370.95
40X	357.4	23.15	380.55
41X	367.1	23.15	390.25
42X	376.7	23.15	399.85
43X	386.3	23.15	409.45
44X	396.0	23.15	419.15
45X	405.6	23.15	428.75
46X	415.2	23.15	438.35
47X	424.8	23.15	447.95
48X	434.5	23.15	457.65
49X	444.1	23.15	467.25
50X	453.8	23.15	476.95
51X	463.4	23.15	486.55
52X	473.1	23.15	496.25

Note: The offsets transform ODP standard depth values in meters below seafloor (mbsf) to meters composite depth (mcd).

22A) over some depth intervals. A zone of high variability in elevated magnetic susceptibility values occurs between 65 and 75 mbsf (Fig. 21B).

GRAPE density and index properties wet bulk density display a high degree of similarity. GRAPE density varies from 1530 kg/m^3 to 1900 kg/m^3. The overall increase in density is caused by compaction. Intermediate variability in GRAPE density may correspond to lithologic boundaries (see "Lithostratigraphy" section, this chapter). Similar to Site 1086, higher values in GRAPE density than in wet bulk density can be observed over the entire depth range at Site 1087.

Velocities

Discrete velocities (Fig. 20) decrease within the upper 10 m from 1600 to 1540 m/s. The higher velocities in the top portion of Hole 1087A may be caused by coarser grained particles (see "Lithostratigraphy" section, this chapter). Below 10 mbsf, velocity values increase in correspondence to GRAPE and index properties wet bulk density values.

Between 0 and 255 mbsf, most of the MST *P*-wave values are lower than the discrete velocities (Fig. 20). Similar to Hole 1086A, much lower gas content was observed at Hole 1087A (see "Organic Geochemistry" section, this chapter), which resulted in less disturbed sediments.

Index Properties

Data from discrete measurements of wet bulk density, porosity, and moisture content are displayed in Figures 22A, 22B, and 22C, respectively (also see Table 12 on CD-ROM, back pocket, this volume). Wet bulk density values vary between 1500 and 1810 kg/m^3, indicating a coarser grain-size distribution in the sediments compared with the clay-rich sediments from other Leg 175 sites.

The wet bulk density profile shows an overall increase which is mostly associated with compaction. Hole 1087A consists mainly of foraminifer-nannofossil ooze (see "Lithostratigraphy" section, this chapter), which is reflected in generally higher values of wet bulk density and velocity.

In general, porosity and moisture profiles are inversely correlated with the wet bulk density. Porosities decrease from 68% in the top section to 53% at 255 mbsf (Fig. 22B). Moisture content varies between 44% at the top of Hole 1087A and 32% at 255 mbsf (Fig. 22C).

Thermal Conductivity and Geothermal Gradient

The thermal conductivity profile (Fig. 21B) at Hole 1087A was measured in every second and fifth core section above 40 mbsf and in every fifth core section below (see "Explanatory Notes" chapter, this volume). Values range between 0.8 W/(m·K) at 22 mbsf and 1.2 W/(m·K) at 50 mbsf. Higher variability in thermal conductivity values can be observed between 0 and 76 mbsf, whereas below 76 mbsf, variations in thermal conductivity are much less pronounced. Similarity between the thermal conductivity profile (Fig. 21B) and magnetic susceptibility exists (Fig. 21A). Thermal conductivity values vary in the same range as those at Sites 1085 and 1086.

At Hole 1087A, the Adara tool was deployed to measure formation temperature. A preliminary analysis provided three data points, which were used to estimate a geothermal gradient of 52°C/km, but further analyses will be required to confirm this result.

Table 9. List of splice tie points used to create the continuous "spliced" stratigraphic sequence for Site 1087.

Hole, core, section, interval (cm)	Depth (mbsf)	Composite depth (mcd)	Whether tied	Hole, core, section, interval (cm)	Depth (mbsf)	Composite depth (mcd)	Offset (m)
1087A-1H-4, 78	5.28	5.28	Tie to	1087C-2H-2, 32	3.46	5.28	1.82
1087C-2H-5, 54	8.14	9.96	Tie to	1087A-2H-1, 39	8.59	9.96	1.37
1087A-2H-7, 34	17.54	18.91	Tie to	1087B-3H-2, 136.5	18.39	18.91	0.52
1087B-3H-4, 104	21.04	21.56	Tie to	1087A-3H-2, 39	19.59	21.56	1.97
1087A-3H-6, 44	25.54	27.51	Tie to	1087C-4H-3, 66.5	24.29	27.51	3.22
1087C-4H-6, 4	28.14	31.36	Tie to	1087A-4H-1, 124	28.44	31.36	2.92
1087A-4H-5, 124	34.44	37.36	Tie to	1087C-5H-3, 2	33.16	37.36	4.20
1087C-5H-6, 134	38.94	43.14	Tie to	1087A-5H-1, 94	37.64	43.14	5.50
1087A-5H-6, 69	44.89	50.39	Tie to	1087C-6H-4, 106.5	45.19	50.39	5.20
1087C-6H-6, 84	47.94	53.14	Tie to	1087A-6H-1, 74	46.94	53.14	6.20
1087A-6H-5, 139	53.59	59.79	Tie to	1087C-7H-3, 106.5	53.19	59.79	6.60
1087C-7H-6, 74	57.34	63.94	Tie to	1087A-7H-1, 89	56.59	63.94	7.35
1087A-7H-6, 4	63.24	70.59	Tie to	1087C-8H-3, 144	63.04	70.59	7.55
1087C-8H-6, 14	66.24	73.79	Tie to	1087B-8H-4, 74	68.24	73.79	5.55
1087B-8H-7, 24	72.24	77.79	Tie to	1087C-9H-1, 74	68.84	77.79	8.95
1087C-9H-7, 4	77.14	86.09	Tie to	1087A-9H-2, 4	76.24	86.09	9.85
1087A-9H-6, 34	82.54	92.39	Tie to	1087C-10H-3, 144	82.04	92.39	10.35
1087C-10H-6, 44	85.54	95.89	Tie to	1087A-10H-1, 84	85.04	95.89	10.85
1087A-10H-5, 134	91.54	102.39	Tie to	1087C-11H-3, 64	90.74	102.39	11.65
1087C-11H-6, 114	95.74	107.39	Tie to	1087A-11H-2, 64	95.84	107.39	11.55
1087A-11H-5, 84	100.54	112.09	Tie to	1087C-12H-2, 104	99.14	112.09	12.95
1087C-12H-6, 54	104.64	117.59	Tie to	1087A-12H-2, 24	104.94	117.59	12.65
1087A-12H-5, 44	109.64	122.29	Tie to	1087C-13H-2, 4	107.64	122.29	14.65
1087C-13H-6, 64	114.24	128.89	Tie to	1087A-13H-2, 34	114.54	128.89	14.35
1087A-13H-6, 64	120.84	135.19	Tie to	1087C-14H-4, 4	120.14	135.19	15.05
1087C-14H-6, 14	123.24	138.29	Tie to	1087A-14H-1, 114	123.34	138.29	14.95
1087A-14H-4, 94	127.64	142.59	Tie to	1087C-15H-2, 4	126.64	142.59	15.95
1087C-15H-6, 14	132.74	148.69	Tie to	1087A-15H-1, 144	133.14	148.69	15.55
1087A-15H-7, 14	140.84	156.39	Tie to	1087C-16H-4, 134	140.44	156.39	15.95
1087C-16H-6, 144	143.54	159.49	Tie to	1087A-16H-2, 24	142.94	159.49	16.55
1087A-16H-6, 74	149.44	165.99	Tie to	1087C-17H-3, 145	148.55	165.99	17.44
1087C-17H-6, 124	152.84	170.28	Tie to	1087A-17H-1, 54	151.24	170.28	19.04
1087A-17H-6, 34	158.54	177.58	Tie to	1087C-18H-4, 104	159.05	177.58	18.53
1087C-18H-6, 114	162.15	180.68	Tie to	1087A-18H-1, 52.5	160.73	180.68	19.95
1087A-18H-5, 124	167.44	187.39	Tie to	1087C-19H-1, 104	164.14	187.39	23.25
1087C-19H-7, 44	172.54	195.79	Tie to	1087A-19H-1, 24	169.94	195.79	25.85
1087A-19H-7, 64	179.34	205.19	Tie to	1087C-21H-1, 0	182.10	205.25	23.15
1087C-21H-6, 124	190.84	213.99					

Note: The tie points are listed in standard ODP meters below seafloor (mbsf) and meters composite depth (mcd).

DOWNHOLE LOGGING

Hole 1087C was planned to be logged with a full suite of sensors to continuously characterize the sedimentary changes, to correlate the lithostratigraphy with other sites, and to provide data for core-log integration. Unfortunately, the logging tool string could not be retrieved after the first run, which ended operations at Hole 1087C (see "Operations" section, this chapter).

Logging Operations

Hole 1087C was logged with one tool string (seismostratigraphy,) which included the NGT, LSS, DIT, and TLT sondes. The logs were run downhole and uphole from 492 mbsf (total depth) to 80 mbsf, where the tool string got stuck at the bottom of the pipe. The natural gamma-ray intensity is the only parameter measurable through the pipe, but it should be interpreted only qualitatively in this interval. The pipe was set at 87 mbsf and pulled up to ~57 mbsf during logging. The wireline logging heave compensator was not used because of rough sea conditions.

Data Quality and General Results

The lithologic succession recovered from Hole 1087C is controlled mainly by changes in the nature and intensity of biogenic production vs. the type and amount of detrital input. It is characterized by small changes in sediment composition and compaction, which should be reflected in the log physical properties measurements. Despite the uniform lithostratigraphy defined from core observations and smear-slide studies (see "Lithostratigraphy" section, this chapter), the good quality and high resolution of the downhole measurements allow us to identify numerous sedimentary changes in the logged formation (Fig. 23).

Lithostratigraphic Unit II at the very bottom of the hole is characterized by higher gamma-ray intensity, resistivity, and acoustic velocity, with a transition which fits with the boundary between lithostratigraphic Units II and I (see "Lithostratigraphy" section, this chapter). In this formation, the acoustic velocity is >2200 m/s for a 2-m-thick interval at ~455 mbsf. Between 350 and 300 mbsf, a progressive decrease in both gamma-ray intensity and resistivity corresponds to the higher carbonate content of the sediment (see "Organic Geochemistry" section, this chapter). Above this depth, the general trend of velocity values mainly reflects downhole compaction and lithification. Uranium content shows a distinct increase uphole, beginning near 200 mbsf and reaching a plateau near 120 mbsf.

Besides these general trends, the 370–350 and 140–120 mbsf intervals are characterized by high values of gamma-ray intensity, resistivity, and uranium content, with drastic excursions for gamma-ray intensity below 300 mbsf. These intervals might reflect abrupt changes in the ratio between clastic and biogenic components, as they show up simultaneously in internal parameters. Diagenesis could enhance or modify such lithologic changes, as suggested by high resistivity and steady velocity values between 370 and 350 mbsf.

Correlation Between Holes 1085A (Mid-Cape Basin) and 1087C (Southern Cape Basin)

The downhole measurements of the two neighboring holes are very similar, despite the higher sedimentation rate observed at Site 1085 in the Mid-Cape Basin. Both general trends and details can be correlated between the two sites, as shown by the gamma-ray intensity (Fig. 24). Despite the higher sedimentation rate, gamma-ray in-

tensity is higher and the amplitude of general shifts is sharper in the Mid-Cape Basin.

REFERENCES

Berggren, W.A., Kent, D.V., Swisher, C.C., III, and Aubry, M.-P., 1995. A revised Cenozoic geochronology and chronostratigraphy. *In* Berggren, W.A., Kent, D.V., Aubry, M.-P., and Hardenbol, J. (Eds.), *Geochronology, Time Scales and Global Stratigraphic Correlation.* Spec. Publ.—Soc. Econ. Paleontol. Mineral. (Soc. Sediment. Geol.), 54:129–212.

Caulet, J.-P., 1991. Radiolarians from the Kerguelen Plateau, Leg 119. *In* Barron, J., Larsen, B., et al., *Proc. ODP, Sci. Results,* 119: College Station, TX (Ocean Drilling Program), 513–546.

Claypool, G.E., and Kvenvolden, K.A., 1983. Methane and other hydrocarbon gases in marine sediment. *Annu. Rev. Earth Planet. Sci.,* 11:299–327.

Cragg, B.A., Harvey, S.M., Fry, J.C., Herbert, R.A., and Parkes, R.J., 1992. Bacterial biomass and activity in the deep sediment layers of the Japan Sea, Hole 798B. *In* Pisciotto, K.A., Ingle, J.C., Jr., von Breymann, M.T., Barron, J., et al., *Proc. ODP, Sci. Results.,* 127/128 (Pt. 1): College Station, TX (Ocean Drilling Program), 761–776.

Martini, E., 1971. Standard Tertiary and Quaternary calcareous nannoplankton zonation. *In* Farinacci, A. (Ed.), *Proc. 2nd Int. Conf. Planktonic Microfossils Roma:* Rome (Ed. Tecnosci.), 2:739–785.

Millero, F.J., and Sohn, M.L., 1992. *Chemical Oceanography:* Boca Raton (CRC Press).

Okada, H., and Bukry, D., 1980. Supplementary modification and introduction of code numbers to the low-latitude coccolith biostratigraphic zonation (Bukry, 1973; 1975). *Mar. Micropaleontol.,* 5:321–325.

Weaver, P.P.E., 1993. High resolution stratigraphy of marine Quaternary sequences. *In* Hailwood, E.A., and Kidd, R.B. (Eds.), *High Resolution Stratigraphy.* Geol. Soc. Spec. Publ. London, 70:137–153.

Ms 175IR-115

NOTE: Core-description forms ("barrel sheets") and core photographs can be found in Section 4, beginning on page 581. Forms containing smear-slide data can be found on CD-ROM. See Table of Contents for materials contained on CD-ROM.

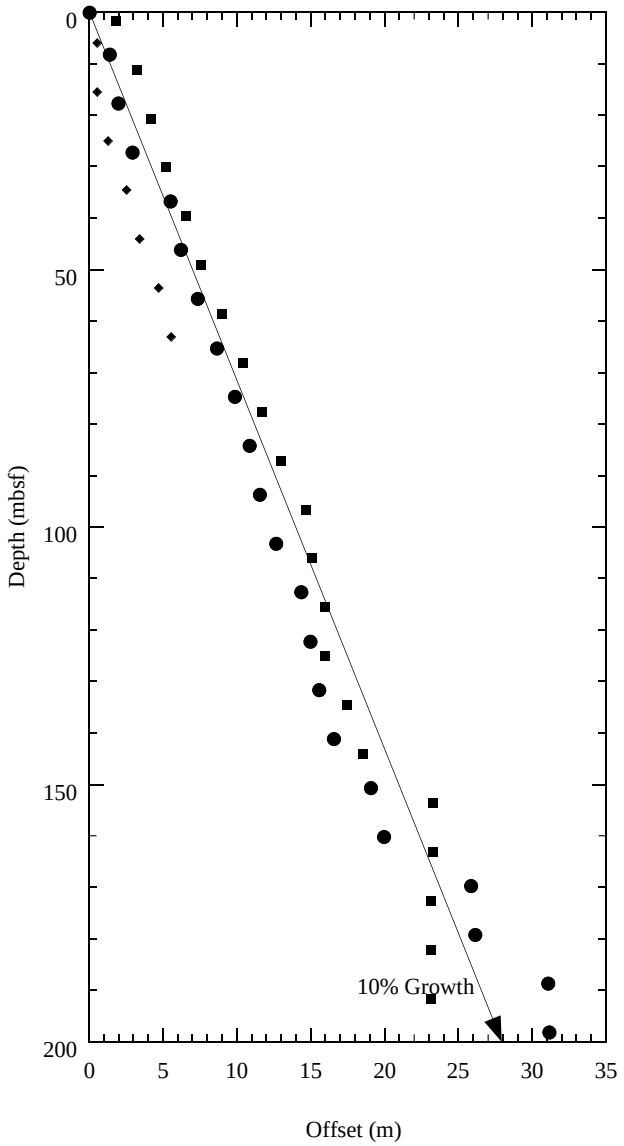

Figure 11. Core offsets applied to Site 1087 plotted against standard ODP meters below seafloor (mbsf). A linear 10% growth of meters composite depth (mcd) compared with mbsf is indicated by an arrow. Offsets are plotted for Holes 1087A (circles), 1087B (diamonds), and 1087C (squares).

Table 10. Interstitial water composition for Holes 1087A and 1087C.

Core, section, interval (cm)	Depth (mbsf)	pH	Alkalinity (mM)	Salinity	Cl^- (titr) (mM)	Cl^- (IC) (mM)	SO_4^{2-} (mM)	Na^+ (mM)	Mg^{2+} (mM)	Ca^{2+} (mM)	K^+ (mM)	H_4SiO_4 (µM)	NH_4^+ (µM)	PO_4^{3-} (µM)
175-1087A-														
1H-1, 140-150	1.40	7.51		35.0	552	546	27.55	471	52.73	9.91	10.63	225	34	11
1H-3, 140-150	4.40	7.32	3.147	35.0	550	552	27.48	466	54.22	10.88	11.76	321	142	16
2H-3, 140-150	12.60	7.58	5.371	35.0	554	544	26.83	471	54.19	10.86	11.54	445	595	19
3H-3, 130-140	22.00	7.72	14.311	34.5	558	550	16.89	476	52.78	6.65	10.76	631	1793	37
4H-3, 140-150	31.60	7.72	18.109	35.0	559	562	13.03	466	52.50	7.43	18.01	605	2429	42
5H-3, 140-150	41.10	7.84	23.866	36.0	555	553	8.90	478	48.32	5.66	11.67	629	3044	48
6H-3, 140-150	50.60	7.85	26.588	37.5	556	548	5.57	483	45.67	4.59	10.37	605	3400	48
7H-3, 140-150	60.10	7.82	28.391	34.0	555	542	3.84	483	44.45	4.31	10.86	618	3746	53
8H-4, 140-150	71.10	7.84	30.145	33.0	556	541	1.02	486	41.93	4.12	10.54	696	4069	69
9H-3, 140-150	79.10	7.71	31.233	33.5	555	543	0.58	485	41.80	4.42	10.87	714	4371	48
10H-3, 140-150	88.60	7.58	30.971	33.5	555	543	0.76	490	39.88	4.34	9.65	696	4371	46
11H-3, 140-150	98.10	6.52	29.839	33.5	553	543	0.36	484	39.36	5.17	10.54	670	4706	43
14H-3, 140-150	126.60	6.83	30.397	33.0	547	539	0.22	479	38.34	6.14	9.85	605	4695	43
17H-3, 140-150	155.10	6.97	26.398	33.0	547	535	0.40	474	38.44	6.82	9.82	525	4911	30
20H-3, 140-150	183.60	6.70	27.110	33.0	547	554	0.84	475	37.89	7.81	9.48	471	4814	20
23H-3, 140-150	212.10	6.71	25.785	32.5	546	542	0.22	482	34.03	7.16	8.34	455	4652	16
26H-3, 140-150	240.60	6.86	22.411	32.0	545	535	0.53	482	32.21	7.19	7.94	414	4296	11
27H-5, 140-150	253.10	6.69	22.542	32.0	546	541	0.43	477	34.04	7.92	7.94	437	4361	13
175-1087C-														
25H-3, 140-150	224.50	6.79	24.806	32.5										
28X-3, 140-150	253.00	6.95	22.461	32.0										
31X-3, 140-150	275.20	6.77	19.151	32.0										
34X-3, 140-150	304.10	6.89	18.168	32.0										
37X-3, 140-150	332.90	6.93	16.176	31.5										
40X-3, 140-150	361.80	7.12	11.624	31.0										
43X-3, 135-150	390.65	7.32	8.268	30.5										
46X-3, 135-150	419.55	7.12	6.389	30.5										
49X-3, 135-150	448.45	7.29	3.362	30.5										
52X-3, 135-150	477.45	7.15	2.134	31.5										

Notes: Cl^- (titr) = analyzed by titration and Cl^- (IC) = analyzed by ion chromatography. Empty cells = not analyzed.

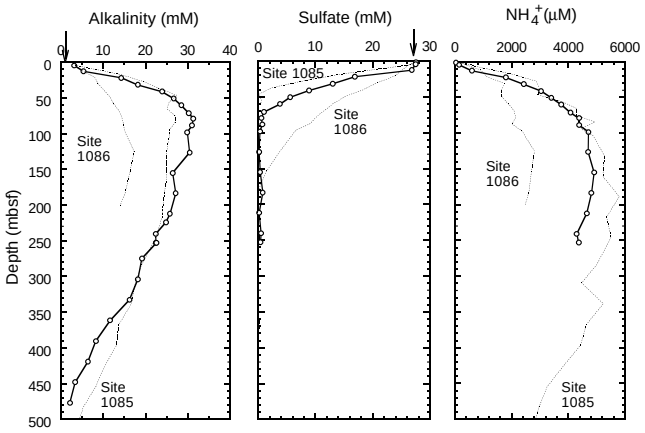

Figure 12. Downcore profiles of dissolved alkalinity, sulfate, and ammonium at Site 1087 (solid lines with open circles). Profiles from Sites 1085 and 1086 (dotted lines) are shown for comparison. Arrows = mean ocean-bottom-water values taken from Millero and Sohn (1992). Note the extended depth scale compared with those in Figures 13, 14, and 15.

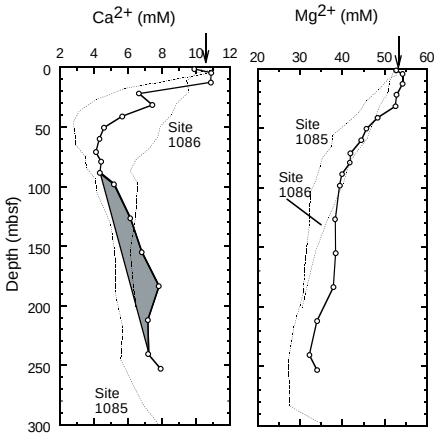

Figure 13. Downcore profiles of Ca^{2+} and Mg^{2+}at Site 1087 (solid lines with open circles). Profiles from Sites 1085 and 1086 (dotted lines) are shown for comparison. Shaded region = depth interval of elevated dissolved Ca^{2+} concentrations. Arrows = mean ocean-bottom-water values taken from Millero and Sohn (1992).

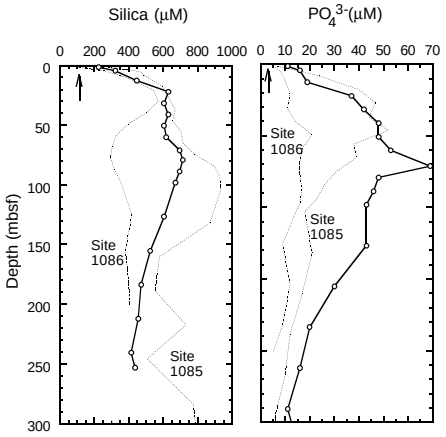

Figure 14. Downcore profiles of dissolved silica and phosphate at Site 1087 (solid lines with open circles). Profiles from Sites 1085 and 1086 (dotted lines) are shown for comparison. Arrows = mean ocean-bottom-water values taken from Millero and Sohn (1992).

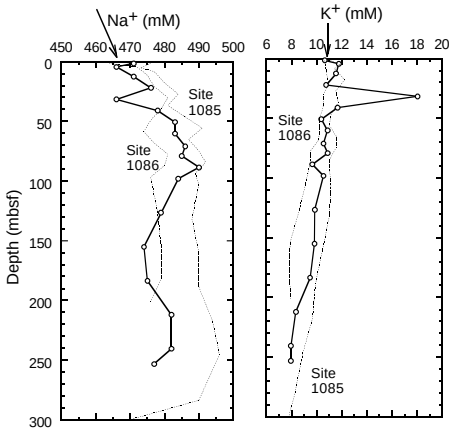

Figure 15. Downcore profiles of dissolved Na^+ and K^+ at Site 1087 (solid lines with open circles). Profiles from Sites 1085 and 1086 (dotted lines) are shown for comparison. Arrows = mean ocean-bottom-water values taken from Millero and Sohn (1992).

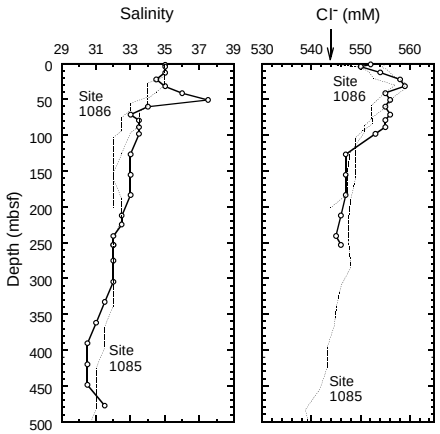

Figure 16. Downcore profiles of salinity and dissolved Cl^- at Site 1087 (solid lines with open circles). Profiles from Sites 1085 and 1086 (dotted lines) are shown for comparison. Arrow = mean ocean-bottom-water value taken from Millero and Sohn (1992). Note extended depth scale compared with those in Figures 13, 14, and 15.

Table 11. Results of headspace gas analyses of sediments from Holes 1087A and 1087C.

Hole, core, section, interval (cm)	Depth (mbsf)	C_1 (ppmv)	CO_2 (ppmv)	C_2= (ppmv)	C_2 (ppmv)	C_3 (ppmv)	C_1/C_2
1087A-1H-2, 0-5	1.50	2	1,266				
1087A-1H-4, 0-5	4.50	3	1,357				
1087A-2H-4, 0-5	12.70	6	3,737				
1087A-3H-4, 0-5	22.10	25	16,520		0.3		93
1087A-4H-4, 0-5	31.70	54	21,675		0.7	0.4	82
1087A-5H-4, 0-5	41.20	68	19,416	0.4	0.7	0.6	98
1087A-6H-4, 0-5	50.70	79	28,958		0.9	0.7	92
1087A-7H-4, 0-5	60.20	78	1,296		0.8	0.6	97
1087A-8H-5, 0-5	71.20	183	25,908		1.0	1.0	192
1087A-9H-4, 0-5	79.20	381	38,386		0.8	0.7	476
1087A-10H-4, 0-5	88.70	897	32,535		1.4	1.6	641
1087A-11H-4, 0-5	98.20	1,241	31,720		1.4	1.6	886
1087A-12H-6, 0-5	110.70	1,171	22,720		1.1	1.2	1,065
1087A-13H-6, 0-5	120.20	1,299	20,255		1.2	1.5	1,082
1087A-14H-4, 0-5	126.70	1,573	22,167		1.4	1.9	1,124
1087A-15H-6, 0-5	139.20	2,064	23,247		1.4	1.9	1,474
1087A-16H-6, 0-5	148.70	2,046	20,390		1.4	1.8	1,461
1087A-17H-4, 0-5	155.20	2,865	26,412		1.5	2.1	1,910
1087A-18H-5, 0-5	166.20	2,153	19,421		1.2	1.5	1,794
1087A-19H-6, 0-5	177.20	2,541	20,980		1.5	2.5	1,694
1087A-20H-4, 0-5	183.70	4,043	29,420	0.2	2.0	2.9	2,022
1087A-21H-6, 0-5	196.20	4,383	26,995	0.2	2.0	2.5	2,192
1087A-22H-5, 0-5	204.20	3,596	19,354		1.4	1.8	2,569
1087A-23H-4, 0-5	212.20	3,636	20,261		1.4	1.6	2,597
1087C-25H-4, 0-5	224.60	2,390	12,177		0.9	1.0	2,656
1087A-24H-6, 0-5	224.70	3,361	16,412		1.1	1.2	3,055
1087A-25H-6, 0-5	234.20	3,473	15,569		1.3	1.7	2,672
1087C-26H-6, 0-5	237.10	2,935	13,106		1.1	1.4	2,668
1087A-26H-4, 0-5	240.70	4,311	17,323		1.3	1.4	3,316
1087C-27H-6, 0-5	246.60	3,550	13,708		1.0	1.1	3,550
1087C-28X-4, 0-5	253.10	4,748	16,501		1.4	1.7	3,391
1087A-27H-6, 0-5	253.20	4,519	15,535		1.2	1.4	3,766
1087C-29X-5, 0-5	260.90	5,300	17,492		1.4	1.5	3,786
1087C-30X-6, 0-5	268.70	5,670	17,037		1.4	1.6	4,050
1087C-31X-4, 0-5	275.30	2,298	7,406		0.4	0.5	5,745
1087C-32X-6, 0-5	287.90	5,685	15,022		1.1	1.2	5,168
1087C-33X-6, 0-5	297.50	3,867	10,094		0.8	0.7	4,834
1087C-34X-4, 0-5	304.20	3,210	9,463		0.7	0.6	4,586
1087C-35X-6, 0-5	316.75	5,894	11,916		1.0	0.8	5,894
1087C-36X-6, 0-5	326.40	5,924	10,644		0.9		6,582
1087C-37X-4, 0-5	333.00	5,712	10,816		0.8	0.7	6,720
1087C-38X-6, 0-5	345.70	8,972	9,666	0.3	1.2	1.2	7,477
1087C-39X-5, 0-5	353.80	7,733	6,565	0.7	1.2	1.4	6,444
1087C-40X-4, 0-5	361.90	7,032	4,624	1.0	1.5	1.4	4,688
1087C-41X-4, 0-5	371.60	14,254	11,463		1.3	0.8	10,965
1087C-42X-5, 0-5	382.70	9,653	8,714		0.9	0.4	11,224
1087C-43X-4, 0-5	390.80	9,580	6,067	0.2	0.9	0.6	10,886
1087C-44X-4, 0-5	400.50	9,143	4,896		0.7	0.4	13,061
1087C-46X-4, 0-5	419.70	16,509	6,886		1.0	0.5	16,509
1087C-47X-4, 0-5	429.30	14,230	3,542		0.7	0.3	20,329
1087C-48X-4, 0-5	439.00	10,791	3,936		0.6	0.2	19,270
1087C-49X-4, 0-5	448.60	10,241	3,362		0.5	0.1	20,482
1087C-50X-2, 0-5	455.30	7,469	746		0.5		14,938
1087C-51X-6, 0-5	470.90	7,907	1,180		0.2		39,535
1087C-52X-4, 0-5	477.60	8,297	990		0.4		20,742
1087C-53X-6, 0-5	490.20	11,927	989		0.5		23,854

Notes: C_1 = methane; CO_2 = carbon dioxide; C_2= = ethene; C_2 = ethane; and C_3 = propane. Dominance of C_1 over C_2 indicates that the gases originate from in situ microbial degradation of organic matter.

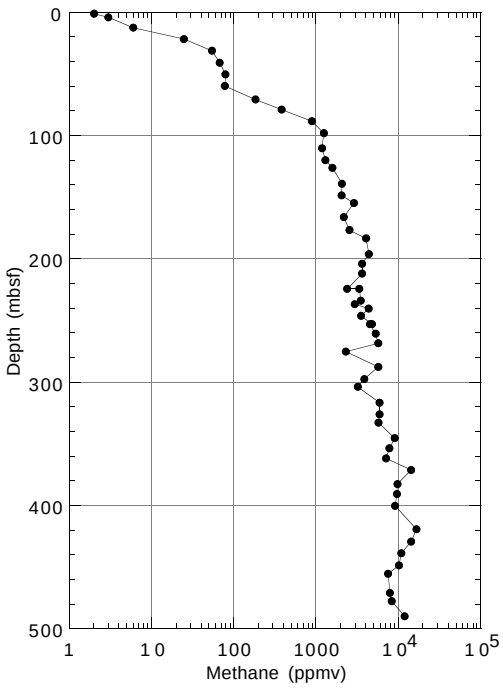

Figure 17. Headspace methane concentrations in sediments from Holes 1087A and 1087C.

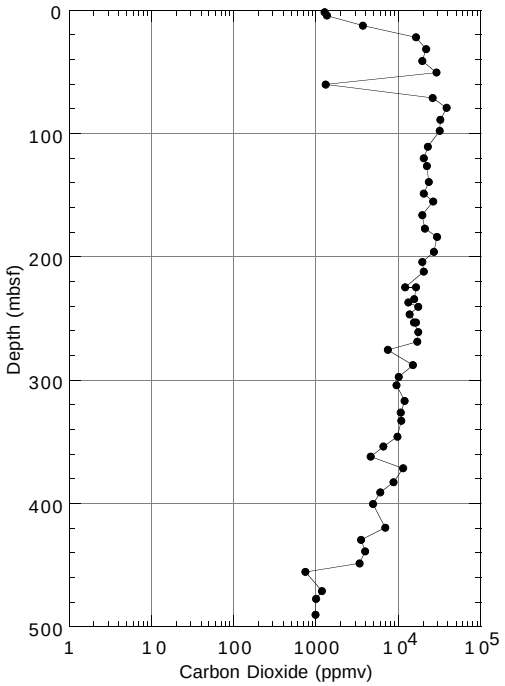

Figure 18. Headspace CO_2 concentrations in sediments from Holes 1087A and 1087C.

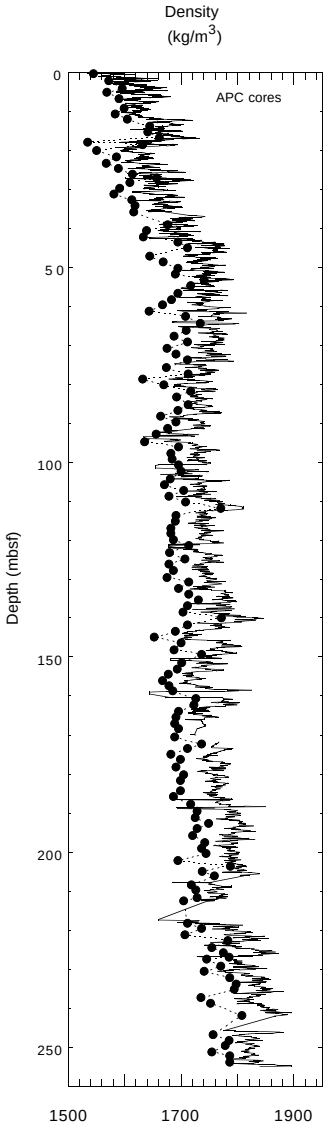

Figure 19. GRAPE wet bulk density data (solid line) superimposed with index properties gravimetric wet bulk density values (solid circles) for Hole 1087A.

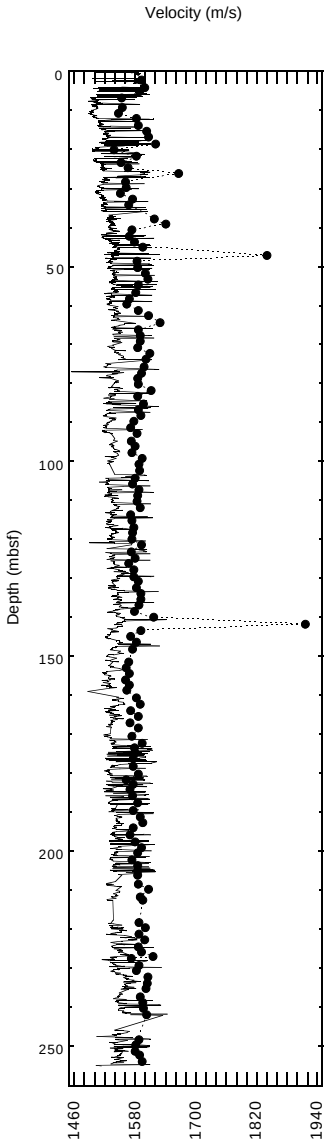

Figure 20. Discrete velocity profile (solid circles) compared with MST velocity data (solid line) measured at Hole 1087A.

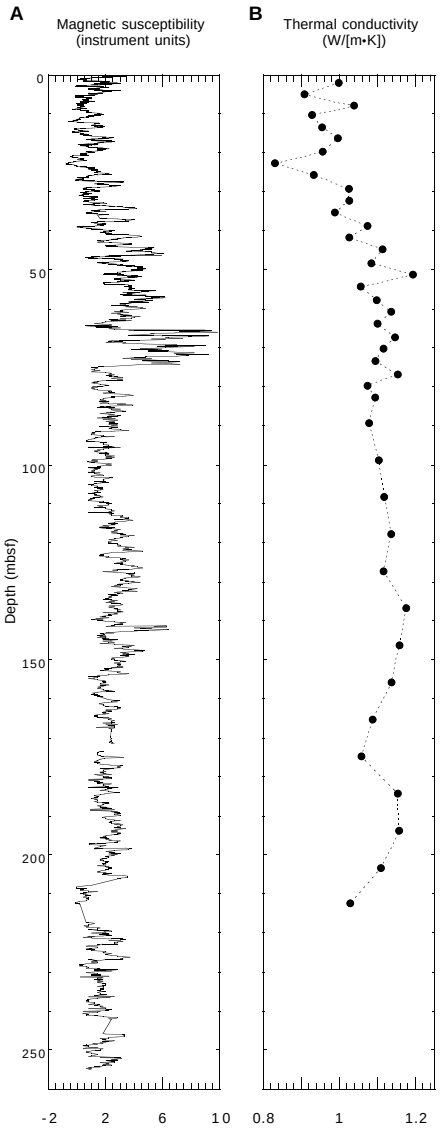

Figure 21. Plots of (**A**) magnetic susceptibility from MST measurements compared with (**B**) discrete values of thermal conductivity between 0 and 255 mbsf at Hole 1087A.

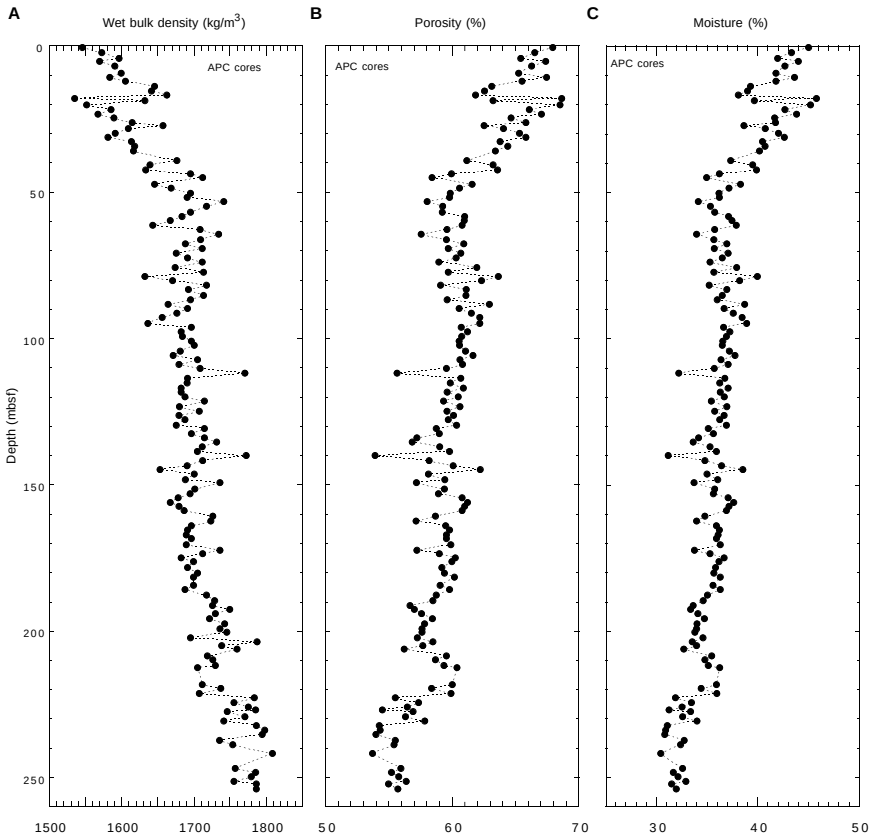

Figure 22. Index properties gravimetric (**A**) wet bulk density, (**B**) porosity, and (**C**) moisture content determined at one sample point per section for Hole 1087A.

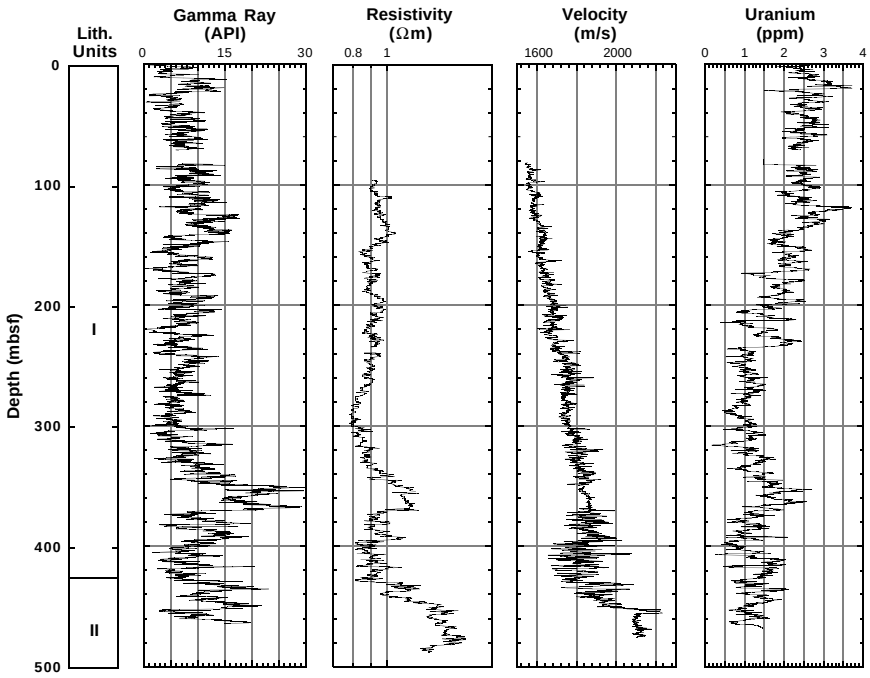

Figure 23. Downhole logs of natural gamma-ray, resistivity, velocity, and uranium content for Hole 1087C.

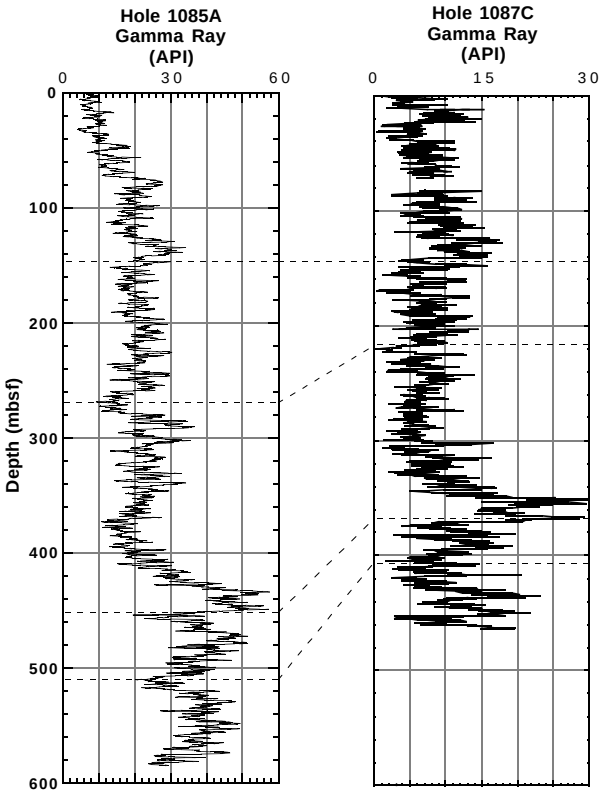

Figure 24. Downhole gamma-ray logs compared between Holes 1085A (Mid-Cape Basin) and 1087C (Southern Cape Basin).